eLife

Reviewed Preprint
v1 • June 17, 2026
Not revised

For correspondence:
liang_lining@gibh.ac.cn
qin_dajiang@gzhmu.edu.cn
zheng_hui@gibh.ac.cn

# These authors contributed equally.

Competing interests: No competing interests declared

Funding: See page 39

Reviewing editor: Bo Gao, The Chinese University of Hong Kong, Hong Kong

The Par complex regulates apical-basal cell polarity through modulation of FAK signaling homeostasis

Meiai He[1,2,3,#], Lining Liang[2,#] ✉, Yulu Wang[2,3], Yongyu Chen[2,4], Hao Sun[2], Lin Guo[2], Changpeng Li[2], Jingcai He[1], Yanhua Wu[2,3], Shiyu Chen[2,3], Tingting Yang[2,3,5], Fei Meng[2,5], Qiwen Ren[2,3], Linna Dong[2,3], Lin Liu[2,3], Qianqian Zou[2,3], Tianya Zhang[2,3], Xinyue Hou[2,3], Qing Guo[2,3], Dajing Qin[1,5] ✉, Hui Zheng[2,3,4,5] ✉

[1]Key Laboratory of Biological Targeting Diagnosis, Therapy and Rehabilitation of Guangdong Higher Education Institutes, The Fifth Affiliated Hospital of Guangzhou Medical University, Guangzhou, China • [2]Guangdong Provincial Key Laboratory of Stem Cell and Regenerative Medicine, Guangdong-Hong Kong Joint Laboratory for Stem Cell and Regenerative Medicine, GIBH-CUHK Joint Research Laboratory on Stem Cell and Regenerative Medicine, Guangzhou Institutes of Biomedicine and Health, Chinese Academy of Sciences, Guangzhou, China • [3]University of Chinese Academy of Sciences, Beijing, China • [4]Joint School of Life Sciences, Guangzhou Medical University, Guangzhou, China • [5]Centre for Regenerative Medicine and Health, Hong Kong Institute of Science & Innovation, Chinese Academy of Sciences, Hong Kong, China

eLife Assessment

This study presents a **valuable** finding that the Par polarity complex, but not Crumbs or Scrib, regulates morphological remodeling during the naive-to-primed transition of pluripotent stem cells, with later effects on differentiation and neural tube organoid lumen formation. The evidence is **incomplete**, as the developmental significance of the PAR KO phenotype requires clearer framing and deeper characterization, and the proposed signaling pathway is currently presented more strongly than the data support. The work will be of interest to developmental and stem cell biologists studying polarity, pluripotent-state transitions, epithelialization, and lumen formation.

https://doi.org/10.7554/eLife.111448.1.sa3

Abstract

Cell polarity complexes are essential for embryogenesis, but their regulatory mechanisms during early developmental transitions remain incompletely understood. Here, we individually deleted the Crumbs, Par, and Scrib polarity complexes in mouse embryonic stem cells (mESCs). While loss of any single complex did not affect pluripotency or proliferation, deletion of Par complex disrupted the naïve-to-primed transition and impaired subsequent differentiation, particularly lumen formation in neural tube organoids. Mechanistically, Par complex deficiency led to hyperphosphorylation of focal adhesion kinase (FAK) at the primed stage, driving a morphological shift from flat monolayer clusters to dome-shaped colonies. FAK inhibition rescued the aberrant morphology. Upstream, Par complex loss increased AKT phosphorylation, which remodeled extracellular matrix (ECM) and regulated integrin signaling via FURIN–LEFTY, ultimately modulating FAK activity. In addition, conditioned medium from wild-type cells partially rescued differentiation defects in Par knockout cells in a LEFTY-dependent manner. These phenotypes were consistently observed in naïve-to-primed transition, neural stem cell differentiation, embryoid body formation, teratoma assays, and neural tube organoid differentiation. Together, these findings establish a Par complex–AKT–FURIN–LEFTY–ECM-integrin–FAK signaling cascade that links apical-basal polarity to early lineage specification and morphogenesis, providing a mechanistic framework for how polarity cues are translated into developmental outcomes.

Graphical Abstract

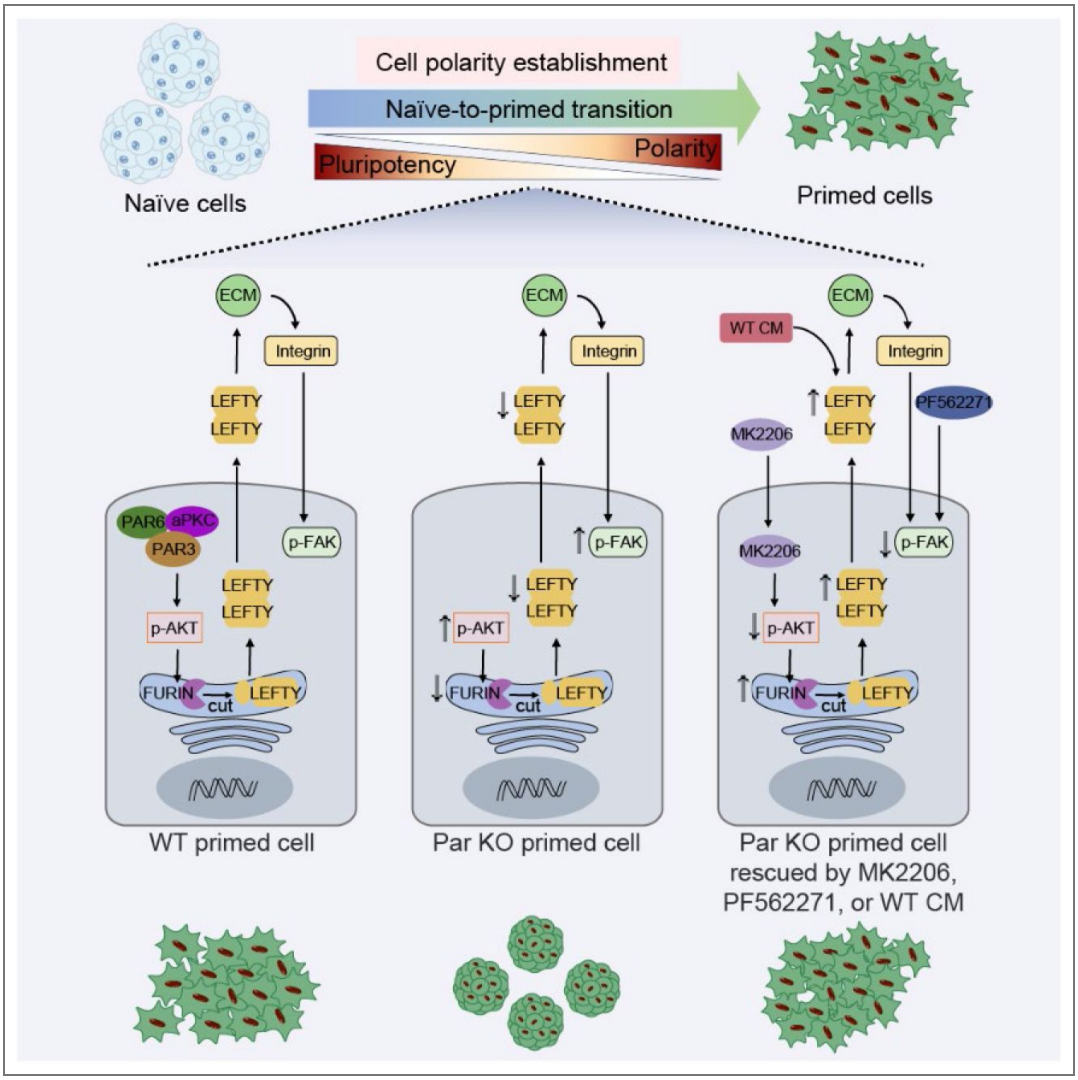

Significance Statement

This study elucidates the molecular mechanism by which the Par complex regulates the establishment of cell polarity. The authors demonstrate that the Par complex promotes the expression of the protein convertase FURIN via AKT signaling, thereby enhancing the maturation and secretion of LEFTY protein. This process remodels the ECM and modulates integrin signaling, ultimately regulating FAK activity and controlling the establishment of cell polarity. These findings reveal how polarity cues govern early lineage specification and morphogenesis, with implications across multiple developmental contexts.

Introduction

The establishment of cell polarity during early embryogenesis represents a fundamental prerequisite of developmental biology, governing embryonic axis formation, cell fate determination, and tissue morphogenesis (Adiyant Lamba, 2025; Leung et al., 2016). In mammals, cell polarity is first established at the morula stage, whereas in non-mammalian species it arises during cleavage stages (Korotkevich et al., 2017; Nelson, 2003). By the 8-cell stage in mice, apical domains begin to form, marking the emergence of apical–basal polarity (Zhu & Zernicka-Goetz, 2020). This process involves the apical localization of conserved polarity complexes such as Crumbs and Par, while the Scrib complex becomes basolaterally enriched to

maintain basal identity (Etemadmoghadam et al., 1995; Watson et al., 2023). The apical domain serves as a platform for recruiting cell fate regulators and encoding lineage-specific markers, thereby guiding lineage specification (Meng Zhu, 2021).

The naïve-to-primed transition (NPT) represents a critical developmental phase in pluripotent stem cells, marked by distinct morphological and molecular changes. Naïve cells maintain dome-shaped colonies and express high levels of pluripotency factors such as *Klf4* and *Esrrb*, whereas primed cells adopt flat monolayer morphology and upregulate lineage-commitment genes including *Brachyury* (*T*) and *Fgf5* (Tesar et al., 2007; Weinberger et al., 2016). Developmentally, naïve state mirrors the pre-implantation inner cell mass, while primed state resembles the post-implantation epiblast (Kalkan et al., 2017). Although naïve cells possess broad differentiation potential, they must transition through the primed state to respond to differentiation signals (Hayashi & Saitou, 2013; Rostovskaya et al., 2019). Primed cells thus represent an intermediate stage between pluripotency and lineage commitment, exhibiting enhanced lineage responsiveness and cell polarity (Brons et al., 2007).

Early studies identified key roles for pathways such as Hippo and AKT in polarity regulation (Tokamov et al., 2023; Xu et al., 2019). More recent interdisciplinary work integrating biomechanical and biomolecular analyses has revealed that extracellular matrix (ECM) and phase separation of polarity proteins collaboratively regulate cell adhesion and migration (Dias Gomes & Iden, 2021; Guzman-Herrera & Mao, 2020). During migration, focal adhesion kinase (FAK) exhibits spatially polarized activity within focal adhesions (Li et al., 2023). FAK amplifies its own activation and membrane localization in response to mechanical or integrin-mediated signals, triggering downstream effectors to promote cell polarity (Diaz-Palacios et al., 2025; Y. Wang et al., 2024). Additionally, active FAK recruits the PI3K–AKT signaling complex to establish a polarity axis and sustain migratory directionality (J. Wang et al., 2024).

Loss of cell polarity is implicated in various human diseases, including neurological disorders, cancer, and tissue fibrosis (Zhan et al., 2008; Zhang & Wei, 2022). In vertebrate embryos, neuroepithelial cells divide predominantly along the apical-basal axis, this polarity is essential for neural tube formation (Herrera et al., 2021). During neural plate folding, epithelial polarization enables neural plate bending, neural fold convergence, and tube closure (Shi, 2022), with polarity proteins mediating intercellular adhesion to maintain structural integrity (Hong et al., 2010; Legere et al., 2024). Neural tube defects (NTDs), including anencephaly caused by *Pard3* deletion, represent severe developmental disorders with high mortality and disability rates, often stemming from failure of embryonic neural tube closure (Chen et al., 2017; Nychyk et al., 2022). Although the molecular basis of NTDs remains incompletely defined, polarity defects in neuroepithelial cells represent a major contributing factor (MacGowan et al., 2025).

In this study, we used CRISPR-Cas9 to knock out Crumbs, Par, and Scrib polarity complexes in mouse embryonic stem cells (ESCs). We systematically characterized polarity abnormalities during differentiation across multiple systems and employed neural tube organoids to investigate how polarity disruption impairs neural tube formation. Our findings uncover key molecular mechanisms through which cell polarity establishes and controls neural tube morphogenesis.

Results

The Par complex is required for morphological remodeling during NPT

To investigate the roles of polarity complexes in cell polarity establishment, we used CRISPR-Cas9 to knock out Crumbs, Par, or Scrib complex in OG2 embryonic stem cells (OG2-ESCs), which represent naïve cells (Figs. 1A and S1A). Two independent knockout cell lines per complex were established and validated for subsequent experiments (Fig. S1B).

We first assessed whether loss of polarity complexes affects pluripotency. Immunofluorescence analysis showed that knockout ESCs maintained normal expression of the pluripotency markers, and 99% of them are Oct4-GFP^{+} (Figs. 1B and S1C). RT-qPCR further confirmed that mRNA levels

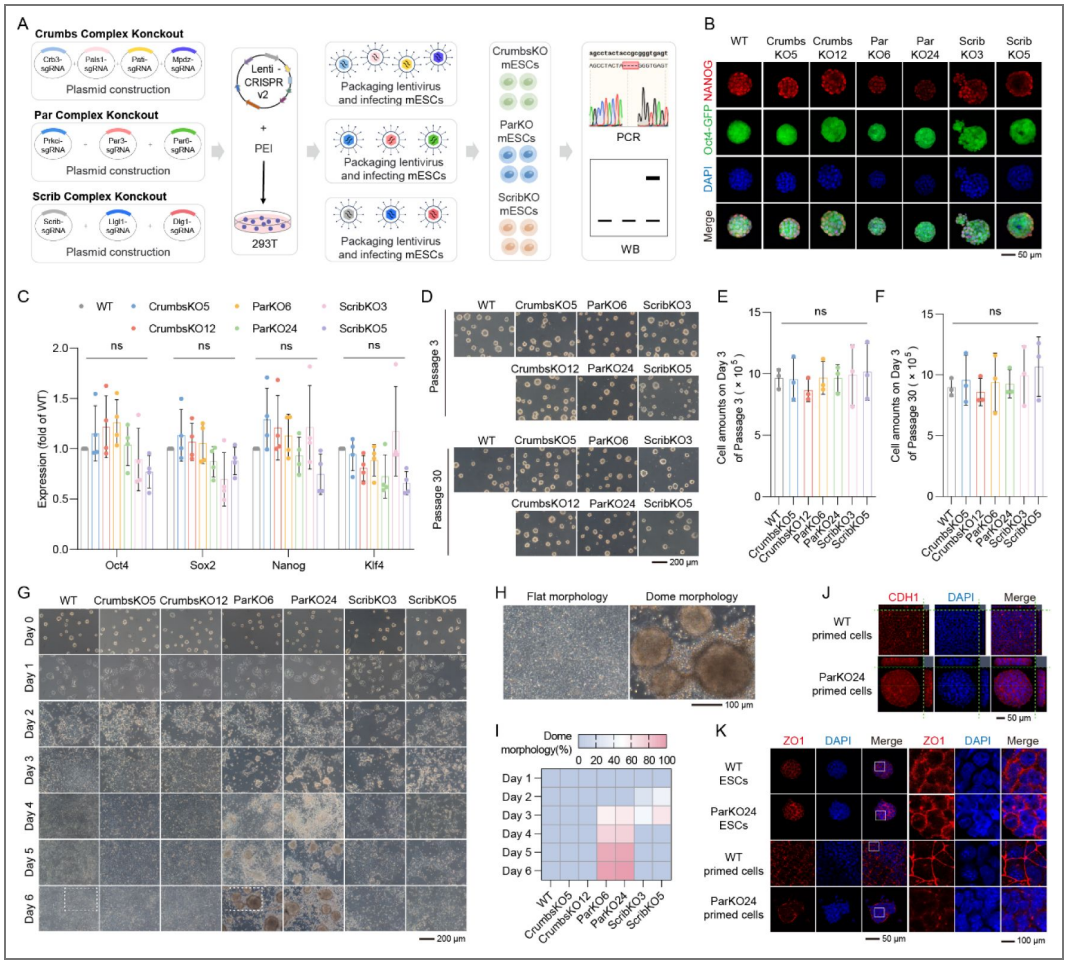

Figure 1. Par complex is essential for NPT.

(A) Schematic illustration of the generation of ESCs without Crumbs, Par, or Scrib complex. **(B-F)** Crumbs, Par, or Scrib complex KO did not affect ESCs pluripotency, morphology, or proliferation. The expression levels of endogenous pluripotency markers *Nanog*, *Oct4*, *Sox2*, and *Klf4* showed no significant differences **(B-C)**. ESCs maintained a characteristic dome-shaped colony morphology over more than 30 passages **(D)**. The initial cell number was 35,000 on day 0, and cell amounts were determined on day 3 **(E-F)**. **(G-I)** Par KO yielded cells exhibiting a dome-shaped colony morphology during NPT, contrasting with the flat monolayer morphology of WT cells. The defining criteria for both morphological types are specified in **(H)**. **(J-K)** Par KO resulted in aberrant subcellular localization of CDH1 and ZO1 in primed cells, as captured by LSM800 confocal microscopy. Experiments were repeated for at least three times unless otherwise mentioned. Error bars represent S.D. Two-way and one-way ANOVA analysis were performed in **(C)** and **(E-F)**, respectively.

of *Oct4*, *Sox2*, *Nanog*, and *Klf4* were not significantly altered in any of the knockout cell lines (Fig. 1C). Moreover, all knockout ESCs retained normal morphology and proliferation capacity after at least 30 passages (Fig. 1D–1F). These results indicate that deletion of polarity complexes does not affect ESC pluripotency.

During NPT process, Par complex knockout cells (ParKO6 and ParKO24) displayed morphology similar to WT cells during the first two days, appearing as a flat monolayer morphology (Fig. 1G). By day 3, however, Par complex knockout (Par KO) cells began to disperse and form dome-shaped colony, a phenotype that became more pronounced over time. By day 6, over 90% of Par KO cells exhibited dome-shaped colonies (Fig. 1G-I). These dome-shaped colonies persisted even after three passages (Fig. S1D-E), indicating a failure to establish epithelial monolayer organization. Live-cell imaging revealed that from day 3 onward, Par KO cells tended to migrate and aggregate into dome-shaped colonies, suggesting day 3 is a crucial time point for the transformation of cell morphology (Vid. 1-2).

In contrast, Scrib complex knockout cells (ScribKO3 and ScribKO5) showed approximately 10% dome-shaped colonies on day 3 of NPT but reverted to flat monolayer clusters by day 6 (Figs. 1G and 1I). Crumbs complex knockout cells (CrumbsKO5 and CrumbsKO12) displayed no notable morphological differences compared to WT throughout NPT (Figs. 1G and 1I). These results establish the Par complex as essential for morphological establishment during NPT. Given the consistent phenotypes in ParKO6 and ParKO24, we focused subsequent studies on ParKO24.

Cell junctions represent hallmark structural features of epithelial polarity, with adherens junctions (marked by CDH1) and tight junctions (marked by ZO1) requiring proper apical polarity for their assembly and function in regulating cell fate (Fleming et al., 1989). To assess junctional organization in our model, we performed immunofluorescence analysis of CDH1 and ZO1 in Par KO primed cells. On day 6 of NPT, CDH1 was localized at the cell-cell junctional membrane in WT primed cells, consistent with its characteristic apical distribution at tight junctions (Yonemura S, 1995), whereas in Par KO primed cells, CDH1 was uniformly distributed around the whole cell membrane without distinct junctional enrichment (Fig. 1J). Additionally, ZO1 showed no significant difference between Par KO and WT ESCs, but its distribution pattern differed significantly in primed cells: WT cells showed strong and continuous ZO1 signal at the apical membrane domain, while Par KO primed cells exhibited weak and scattered staining distributed along the plasma membrane (Fig. 1K). These findings demonstrate that the Par complex is essential for proper junctional organization and polarity establishment during NPT.

The Par complex regulates morphological remodeling through the AKT and FAK signaling pathways

To elucidate the molecular mechanisms by which the Par complex regulates cell polarity establishment, we performed RNA-seq on WT and Par KO cells at five time points (days 0, 1, 3, 4, and 6) during NPT (Fig. 2A). Heatmap analysis revealed that transcriptomic profiles of Par KO cells progressively diverged from WT from day 3 onward, which is consistent with the onset of morphological differences (Figs. 2B and S2A).

Pseudotime analysis indicated that major transcriptional shifts occurred at days 1 and 3 in both genotypes. The overall differentiation trajectory of Par KO cells resembled that of WT, consistent with their ability to upregulate primed markers (Fig. 2C). However, Par KO cells exhibited a slower differentiation progression from day 4, suggesting that polarity loss delays developmental transitions (Fig. 2C). The number of differentially expressed genes (DEGs) between Par KO and WT cells increased over time, with 945 downregulated and 948 upregulated genes in Par KO primed cells at day 6 (Fig. S2A). KEGG analysis revealed that downregulated genes were enriched in focal adhesion, Hippo signaling, PI3K-AKT signaling, cytoskeleton regulation, cell junction, and ECM-receptor interaction (Fig. 2D). Key genes in these pathways, including AKT and FAK, showed differential expression as early as day 3, and the differences gradually increased as NPT proceeded (Figs. 2E and S2B).

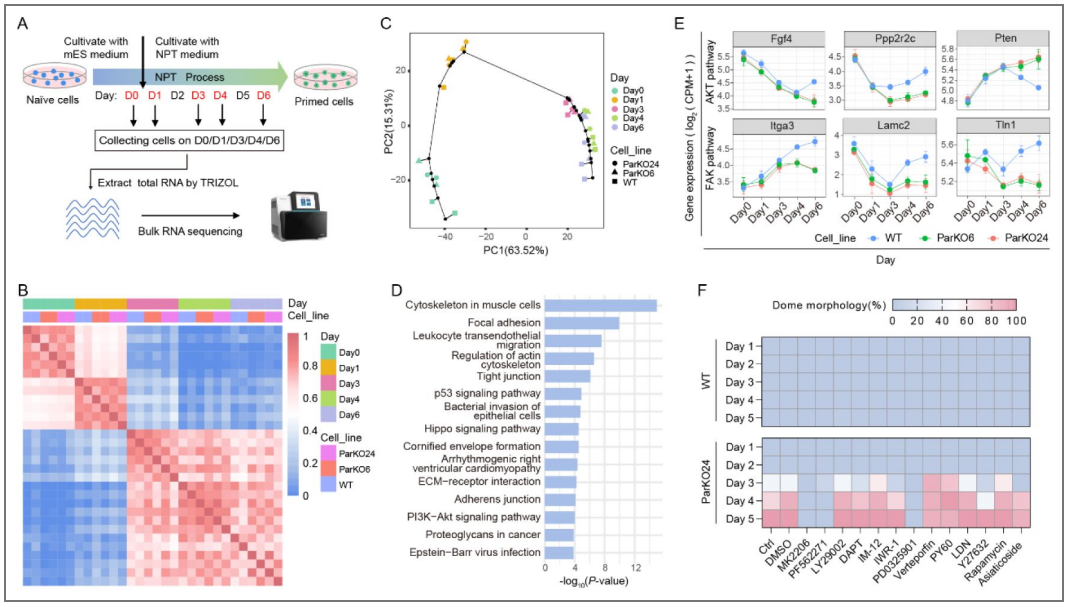

Figure 2. Suppression of AKT or FAK signaling rescues the defect induced by Par KO.

(A) Schematic illustration of RNA-seq analysis. Cells on day 0, 1, 3, 4, and 6 during NPT were collected for bulk RNA-seq during NPT. **(B)** Analysis of intercellular correlations revealed that the transcriptomic differences between Par KO and WT cells became progressively more significant as NPT proceeded. **(C)** Pseudotime analysis of the NPT process revealed that the differentiation progress of Par KO was slower than that of WT starting from day 4, with the difference reaching its maximum on day 6. **(D)** GO analysis of enriched pathways of DEGs on day 6. **(E)** Expression of key genes of the enriched pathways in (D) was analyzed, also see Figure S2B. **(F)** Cells were treated with agonists or inhibitors targeting the enriched pathways during NPT, followed by morphological analysis of dome-shaped colonies. Experiments were repeated for at least three times, with the exception of high-throughput sequencing, or if unless otherwise mentioned. Error bars represent S.D.

Given the broad signaling alterations, we screened small-molecule modulators of these pathways during NPT. The concentrations of small-molecule modulators were optimized based on the recommended IC50 for cell experiments to ensure no significant effects on cell proliferation or apoptosis. Among the compounds tested, only MK2206 (AKT inhibitor) and PF562271 (FAK inhibitor) rescued the morphology defects in Par KO primed cells, restoring flat monolayer clusters (Figs. 2F and S2C). No rescue was observed with compounds targeting PI3K, mTOR, Rho/ROCK, Wnt/β-catenin, Notch, BMP, TGF-β, or Hippo signaling.

Notably, Par KO primed cells treated with PD0325901 (MEK inhibitor) displayed a morphology distinct from both the flat monolayer clusters of typical primed cells and the dome-shaped colonies of naïve cells. Instead, they formed multi-layer clusters characterized by a central dome-shaped region surrounded by peripheral flat cells, exhibiting a more compact and aggregated architecture. (Fig. S2C). Further detection revealed that Par KO primed cells treated with PD0325901 retained high percentage of Oct4-GFP^{+} cells (Fig. S2D) and expressed high levels of *Esrrb* and *Klf4* (Fig. S2E). Consistent with prior reports that PD0325901 sustains pluripotency and prevent ESC differentiation (Ying et al., 2008), these results suggest that the observed "rescue" only reflects a morphological improvement, with a maintenance of the ESC state which hindered NPT progression.

In contrast, treatment with MK2206 or PF562271 fully restored the flat monolayer morphology and normalized gene expression to patterns similar to WT. This was evidenced by comparable levels of primed markers, suppression of ESC markers, and downregulation of endogenous Oct4 (Fig. S2D-S2E). Together, these results indicate that inhibition of AKT or FAK signaling specifically rescued both morphological and molecular defects resulting from Par complex loss during NPT.

Conditioned medium from WT cells rescues the defects induced by Par KO

While the spatiotemporal dynamics of polarity complexes play a pivotal role in directing cell fate specification and lineage differentiation, how their mislocalization or dysregulation in individual cells perturbs embryogenesis remains unclear. To address this, we performed NPT in co-culture systems containing both WT and Par KO ESCs. When cultured alone, Par KO ESCs consistently exhibited dome-shaped colonies. In contrast, co-culture with WT ESCs at initial ratios of 1:1 or 2:1 (Par KO:WT), over 90% cells exhibited flat monolayer clusters (Fig. S3A-S3B). This rescue could be attributed to either the exclusion or the active correction of Par KO cells by WT cells.

To distinguish these possibilities, we established tdTomato-labeled Par KO ESCs and co-cultured them with WT ESCs. When cultured alone, over 92% Par KO primed cells were tdTomato^{+} (Fig. 3A-B), but they proliferated slower than WT primed cells, as the cell amounts of Par KO primed cells was approximately 82% of WT (Fig. 3C). When Par KO and WT ESCs were co-cultured at ratios of 1:1 and 2:1, approximately 24% and 42% tdTomato^{+} cells were observed at the end of NPT (Fig. 3B), marking actual percentage of Par KO primed cells was 26% and 46% (Fig. 3D), which suggested significant survival of Par KO cells with approximately 63% and 84%. Thus, high percentage of flat morphology was possibly due to the active correction of the Par KO phenotype by WT cells.

On the other hand, the proliferation of Par KO cells was impaired in co-culture systems. Given the proliferation rates of Par KO and WT cells when culture alone, the expected percentages of Par KO cells should be approximately 41% and 55% in 1:1 and 2:1 ratio system respectively (Fig. 3D). Reductions around 37% (1:1) and 16% (2:1) suggested that although WT cells rescued the morphology of Par KO cells, they also competed with and impaired the growth of Par KO cells. Compared to the proliferation efficiency in culture alone (approximately 49-fold), the relative proliferation efficiency of WT cells in co-culture systems increased to approximately 69-fold (1:1) and 75-fold (2:1); whereas the proliferation efficiency of Par KO cells decreased from 40-fold in culture alone to 24-fold (1:1) and 32-fold (2:1) in co-culture systems (Fig. 3E).

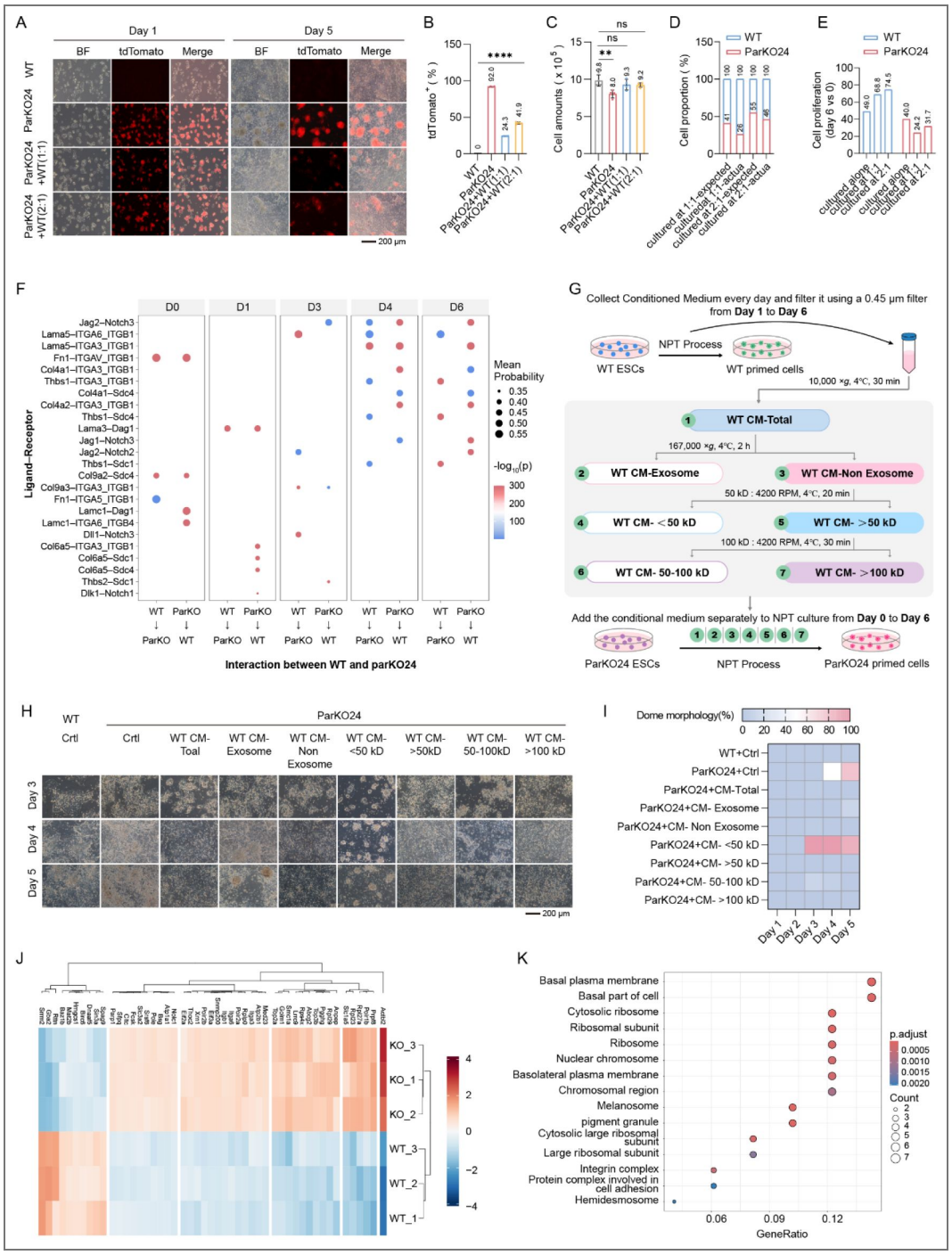

Figure 3. Conditioned medium from WT cells rescues the defect induced by Par KO.

(A-C) tdTomato-labeled Par KO ESCs were co-cultured with WT ESCs during NPT (cell number was 20,000 on day 0). Cell amounts and the proportion of tdTomato$^+$ were determined on Day 6. **(D-E)** Based on the results from (B and C), the proportion of WT and Par KO cells in the co-culture systems was calculated, along with the proliferation efficiency of WT and Par KO cells. **(F)** Analysis of interactions between Par KO and WT cells using RNA-seq data. **(G)** Schematic illustration of component separation of WT CM. The total WT CM was separated into 7 groups. **(H-I)** Different components of WT CM were used to treat the Par KO cells respectively, and the cell morphology were analyzed. **(J-K)** Protein profile was conducted on WT and Par KO CM to analyze the differentially expressed proteins and their signaling pathways. Experiments were repeated for at least three times unless otherwise mentioned. Error bars represent S.D. One-way ANOVA analysis was performed in **(B-C)**.

These findings may reveal a developmental compensation mechanism during embryogenesis: when individual cells exhibit developmental abnormalities with mislocalization or dysregulation of Par complex, normal cells will either actively rescue the defective phenotypes of abnormal cells or increase their own population proportion to dilute the relative abundance of impaired cells, thereby maximizing the probability of normal embryonic development. Analysis of cell-cell interactions during NPT in WT and Par KO cells revealed that the predominant interactions were associated with LAMININ and COLLAGEN pathways, exemplified by receptor-ligand pairs such as *Lama5–Itga6*/*Itgb1*, *Lama5–Itga3*/*Itgb1*, and *Col4a1–Itga3*/*Itgb3* (Fig. 3F). These interactions were notably strengthened between day 4 and day 6 and suggested that Par complex regulates ECM assembly and provides mechanical cues along with integrin-mediated signaling, thereby promoting cell polarization and morphology.

We next asked whether the abilities of WT cells to rescue the morphology of Par KO cells requires direct contact or is mediated by secreted factors. Conditioned medium (CM) from WT cells during days 1–6 of NPT—but not from Par KO cells or WT primed cell lysates (CL)—fully restored flat monolayer morphology in Par KO primed cells (Fig. S3C-S3D). This effect was dependent on sustained exposure, WT CM had to be applied at least from day 1 to day 4 of NPT to achieve complete rescue; and WT CM collected at day 0 of NPT showed no rescuing activity. (Fig. S3E).

To identify the key components in WT CM, we fractionated WT CM into exosome and soluble content, and the soluble content was further separated by molecular weight (Fig. 3G). All the fractions were used to treat Par KO cells during NPT. The rescue activity was retained in groups of WT CM-Total, WT CM-Non exosome, WT CM- > 50 kDa, and WT CM- > 100 kDa (Fig. 3H-I). Although the 50–100 kDa fraction also eventually rescued the phenotype, its effect was delayed, indicating that the key factor(s) reside in the > 100 kDa fraction. Furthermore, the WT CM-Exosome exhibited limited rescue efficacy, particularly during the later stages of NPT. Comparative proteomic profiling of WT and Par KO CM (the > 100 kDa fractions) revealed that WT CM was enriched in proteins involved in cell organization, integrin, and cell adhesion (Fig. 3J-K). These findings suggest that WT cells secrete high-molecular-weight proteins or complexes that restore polarity and morphology in Par KO cells.

The Par complex regulates morphological remodeling through an AKT–FURIN–LEFTY–ECM–integrin–FAK signaling axis

To determine whether AKT inhibition and WT CM share a common rescue mechanism, we performed RNA-seq on Par KO primed cells treated with either MK2206 or WT CM at day 6 of NPT. Clustering analysis demonstrated that both treatments shifted the transcriptional profiles of Par KO primed cells toward the WT pattern, showing clear separation from untreated Par KO controls (Fig. 4A). Compared to Par KO primed cells, 787, 509 and 585 genes were upregulated in WT, MK2206-and WT CM-treated cells respectively. Among these, 302 genes were commonly upregulated under both rescue conditions, indicating substantial mechanistic overlap (Fig. 4B). A core set of 198 genes was upregulated across all three groups (WT, MK2206, and WT CM) compared to Par KO. KEGG analysis revealed that these 198 genes were primarily enriched in pathways related to cytoskeleton, focal adhesion, and ECM-receptor interaction (Fig. 4C), suggesting that both MK2206 and WT CM rescue morphological defects by regulating cell adhesion and ECM-related processes.

Considering that MK2206 is an AKT inhibitor, we measured phosphorylated AKT (p-AKT) levels across different groups. Par KO led to upregulated p-AKT levels, and this increase was effectively suppressed by MK2206 treatment (Fig. S4A). Notably, treatment with WT CM did not decrease p-AKT levels, suggesting WT CM might perform rescue function downstream of AKT signaling. The FAK signaling pathway serves as a central node that integrates upstream inputs from both PKC and AKT pathways, while transducing extracellular cues derived from ECM-integrin interactions into intracellular signaling cascades (Sakthivel et al., 2025). Its enrichment here suggests a central role in rescuing Par KO cell morphology (Fig. 4C). Consistent with this, expression of the focal adhesion proteins *Actn1* and *Flnb*, the integrin *Itga5*, and the ECM regulator *Thbs1* was

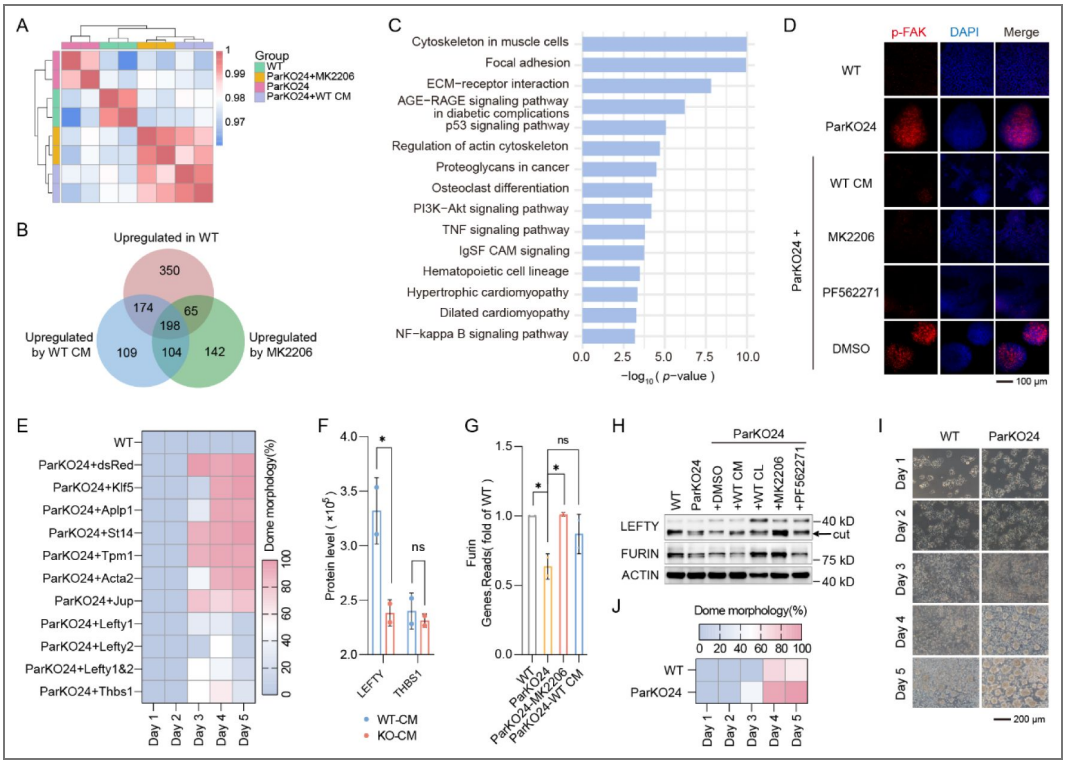

Figure 4. The AKT–FURIN–LEFTY–ECM–integrin–FAK signaling axis mediates Par complex-dependent morphological remodeling.

(A) Analyzed the transcriptome patterns of Par KO primed cells treated with MK2206 and WT CM on Day 6 during NPT. **(B)** Overlap analysis was performed on the upregulated genes from three comparisons: WT versus Par KO, MK2206- or WT CM-treated Par KO versus untreated Par KO. **(C)** KEGG analysis was then conducted on the 198 commonly upregulated genes in **(B)**. **(D)** Par KO ESCs were treated with WT CM, MK2206, or PF562271 respectively during NPT, the p-FAK level in the cells was detected on Day 6. **(E)** Target proteins were overexpressed individually in Par KO ESCs, followed by subjecting the overexpressing ESCs to NPT and analyzing their cell morphology. **(F)** Analyzed the levels of LEFTY and THBS1 in WT and Par KO CM using proteomic data. **(G)** Par KO ESCs were treated with MK2206 or WT CM respectively during NPT, and the *Furin* mRNA expression was detected on Day 6. **(H)** Par KO ESCs were treated with WT CM, MK2206, or PF562271 respectively, and the protein level of the LEFTY and FURIN was detected. The position indicated by the arrow represents the LEFTY cut by FURIN. **(I-J)** Cell morphology of WT and Par KO cells treated with *Furin* inhibitor (BOS318) during NPT. Experiments were repeated for at least three times unless otherwise mentioned. Error bars represent S.D. Two-way and one-way ANOVA analysis were performed in **(F)** and **(G)**, respectively.

significantly reduced in Par KO primed cells at day 6 of NPT (Fig. S4B). Importantly, FAK signaling was hyperphosphorylated in Par KO primed cells compared to WT primed cells, yet both MK2206 and WT CM effectively reduced phosphorylated FAK (p-FAK) levels (Fig. 4D).

The FAK inhibitor PF562271, which significantly rescued the NPT defects caused by Par KO, effectively reduced p-FAK levels in Par KO primed cells (Fig. 4D). Given that both MK2206 and WT CM also attenuated the elevated p-FAK, we propose that all three treatments restore the flat monolayer morphology in these cells by regulating FAK signaling homeostasis.

Through integrated analysis of proteomic and RNA-seq data, we identified a set of functional proteins associated with the FAK signaling (Fig. S4C). These candidate proteins were subsequently overexpressed in Par KO ESCs. Overexpression of LEFTY1, LEFTY2, or THBS1 in Par KO ESCs significantly rescued cell morphology during NPT, with LEFTY1 and LEFTY2 showing the strongest effects (Figs. 4E and S4D). Actually, the protein levels of LEFTY were significantly higher in WT CM compared to KO CM (Fig. 4F), suggesting that WT cells modulate FAK signaling via secretion of LEFTY proteins. Under these conditions, WT CM treatment supplied extracellular LEFTY to Par KO ESCs, thereby rescuing the phenotypic defects of Par KO primed cells. It is therefore reasonable to infer that MK2206 rescues the defects in Par KO primed cells through upregulation of LEFTY expression, which in turn suppresses p-FAK. Concordantly, LEFTY overexpression reduced p-FAK in Par KO primed cells (Fig. S4E), consistent with reported roles of LEFTY in suppressing FAK signaling (Alowayed et al., 2016). These results demonstrate that MK2206 and WT CM rescue morphological defects by suppressing excessive p-FAK through LEFTY.

The intracellular LEFTY proprotein requires proteolytic cleavage by FURIN in the Golgi apparatus to be secreted extracellularly as a stable homodimer, which then exerts its biological function (Dubois et al., 2001). To investigate whether MK2206 influence FURIN expression, we analyzed transcriptomic data and found that Par KO downregulated Furin mRNA expression, whereas MK2206 treatment restored its transcript levels in Par KO cells (Fig. 4G). Consistent with this, MK2206 also increased FURIN protein abundance, consequently enhancing the production of cut LEFTY protein (Fig. 4H). To further validate the essential role of FURIN-mediated cleavage of LEFTY, we treated both WT and Par KO ESCs with BOS318, a highly specific and potent inhibitor of FURIN that irreversibly binds to the protease by mimicking its natural substrate (Ivachtchenko et al., 2024). BOS318 treatment induced WT primed cells to adopt a dome-shaped morphology resembling that of Par KO primed cells (Fig. 4I-J), demonstrating that inhibition of FURIN proteolytic activity by BOS318 prevents the secretion and functional maturation of LEFTY, thereby abrogating its ability to suppress p-FAK and leading to aberrant primed cell morphology.

Following its secretion into the extracellular space, how does LEFTY regulate intracellular p-FAK homeostasis? Integrated analysis of both transcriptomic and proteomic data revealed that Par KO leads to significant enrichment of pathways associated with ECM and integrin (Figs. 2D, 3F, 3K, and S4B). Notably, both MK2206 and WT CM treatment co-upregulated the ECM-receptor interaction pathway (Fig. 4C). We therefore propose that secreted LEFTY acts as an extracellular signal that activates specific ECM receptors and modulates integrin complexes. This in turn regulates FAK phosphorylation, thereby maintaining normal cell adhesion and morphology.

These findings collectively demonstrate that Par complex suppresses p-AKT to upregulate FURIN expression. Following FURIN-mediated proteolytic maturation, LEFTY is secreted and triggers the conversion of ECM-integrin signaling into intracellular cues, which subsequently regulate FAK signaling homeostasis and promote cell polarity establishment.

The Par complex is required for differentiation across multiple developmental contexts via the AKT–FAK signaling axis

Given that Par complex loss disrupts cell morphology during NPT, we asked whether it also impairs multi-lineage differentiation. We differentiated WT ESCs, Par KO ESCs, WT primed cells, and Par KO primed cells into embryoid bodies (EBs) using suspension culture. On day 6, EBs derived from four types of cells formed spherical structures with comparable morphological characteristics (Fig. 5A).

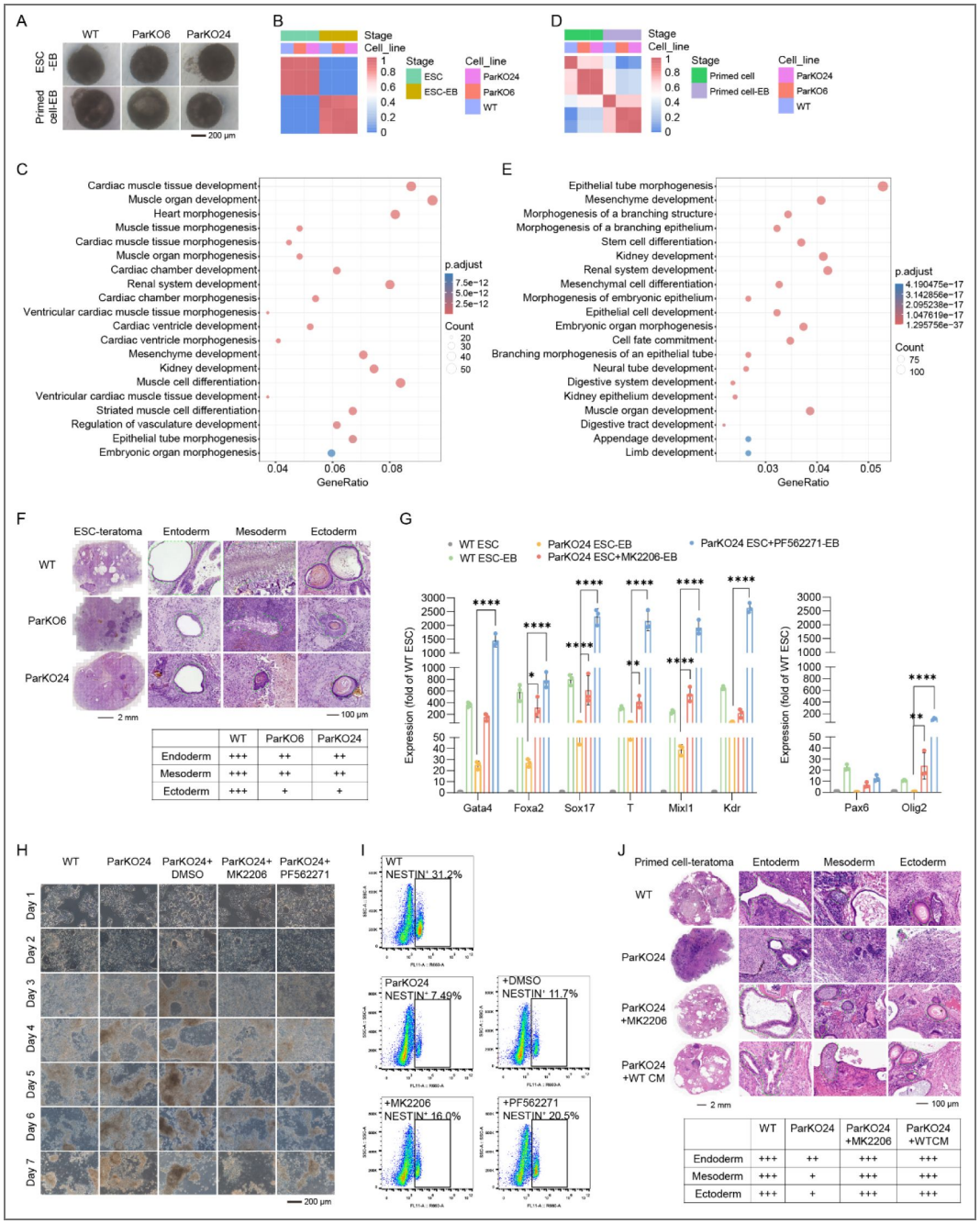

Figure 5. Par KO impairs lineage differentiation via the AKT–FAK signaling axis.

(A) WT ESCs, Par KO ESCs, WT primed cells, and Par KO primed cells were subjected to EB differentiation via suspension culture. **(B-E)** Transcriptome profiling was performed on day 6 of EB differentiation separately for ESC-EBs (WT vs Par KO) and primed cell-EBs (WT vs Par KO). **(F)** Teratomas were generated by subcutaneous injection of WT and Par KO ESCs into immunodeficient mice, followed by histological assessment via H&E staining. H&E-stained sections were imaged by using the TG Tissue FAXS Plus ST. **(G)** Par KO ESCs were treated with MK2206 or PF562271 during EB differentiation, and the expression of three germ layers markers were detected. **(H-I)** Par KO ESCs were treated with MK2206 or PF562271 during the NSC differentiation. The proportion of NESTIN^{+} cells were detected by using the CytoFLEX. **(J)** Subcutaneous injection of WT, Par KO, MK2206- or WT CM-treated Par KO primed cells into immunodeficient mice to form teratoma, followed by H&E staining for histological assessment. Experiments were repeated for at least three times unless otherwise mentioned. Error bars represent S.D. Two-way ANOVA analysis was performed in **(G)**.

Transcriptomic profiling identified WT and Par KO ESC-EBs exhibited significant transcriptional differences (Fig. 5B). GO analysis of DEGs revealed significant enrichment in biological processes related to cardiac muscle tissue development, kidney development, epithelial tube morphogenesis, and embryonic organ morphogenesis when comparing WT with Par KO ESC-EBs (Fig. 5C). Transcriptomic divergence was already established between WT and Par KO primed cells as described previously (Fig. 2D) and persisted during EB differentiation (Fig. 5D). Consistently, DEGs identified between WT and Par KO primed cell-EBs were significantly enriched in epithelial tube morphogenesis, embryonic organ morphogenesis, cell fate commitment, and neural tube development (Fig. 5E). These results collectively demonstrate that Par KO disrupts embryonic development and lineage differentiation processes in ESCs.

To further determine the differentiation preference of Par KO ESCs, we cultured Par KO ESC-EBs for extended period. On day 15 of EB differentiation, RT-qPCR analysis revealed significantly reduced expression of markers representative of all three germ layers in Par KO ESC-EBs compared to WT controls. These included endodermal markers (*Sox17*, *Gata4*, *Foxa2*), mesodermal markers (*Kdr*, *T*, *Mixl1*), and ectodermal markers (*Pax6*, *Olig2*) (Fig. S5A), collectively indicating impaired lineage specification capacity in the absence of Par complex.

We selected ESCs as the starting cell population for the teratoma formation assay to determine whether Par KO affects lineage differentiation *in vivo*. Both WT and Par KO ESCs formed teratomas within four weeks. However, histological analysis by H&E staining revealed that Par KO ESC-derived teratomas exhibited markedly reduced diversity and abundance of tissues representing all three germ layers (Fig. 5F). The most pronounced reduction was observed in ectodermal derivatives, particularly squamous epithelium and pigment cells. This was followed by significant decreases in endodermal lineages, including respiratory epithelium and glandular structures, as well as mesodermal derivatives such as osteoblasts.

Given the pronounced ectodermal defect, we assessed neural stem cell (NSC) differentiation. Par KO ESCs failed to form typical rosette structures (Fig. S5B), and flow cytometry showed a significant reduction in NESTIN$^+$ cells compared to WT ESCs (Fig. S5C). These findings suggest that loss of the Par complex disrupts polarity-driven morphogenesis essential for lineage maturation, particularly in ectodermal derivatives. During EB differentiation, MK2206 and PF562271 treatment robustly enhanced germ layer differentiation in Par KO ESCs. (Figs. 5G and S5D). Similarly, during NSC differentiation, MK2206 and PF562271 treatment rescued NSC morphology (Fig. 5H) and increased the proportion of NESTIN$^+$ cells (Fig. 5I). In the teratoma assay, due to the considerable technical challenges associated with direct *in vivo* administration of compounds or WT CM, we adopted an alternative pre-treatment strategy. Specifically, Par KO ESCs were treated with either MK2206 or WT CM during NPT to generate correspondingly treated primed cells for subsequent *in vivo* assessment. Both MK2206 and WT CM treatment restored tissue organization and germ layer representation in Par KO teratomas to levels comparable with WT controls, as evidenced by the robust presence of mesodermal derivatives such as osteoid tissue and ectodermal lineages including squamous epithelium (Fig. 5J).

Together, these results indicate that Par complex deficiency disrupts lineage specification and NSC generation, and that these defects can be functionally rescued by inhibiting AKT–FAK signaling.

The AKT–FAK signaling axis mediates neural tube organoid defects in Par KO ESCs

Par complex dysfunction is known to cause neural tube closure defects during embryonic development (Chen et al., 2017). In this study, our ESC differentiation assays revealed that Par KO most severely impaired ectodermal lineage specification. To examine the role of the Par complex in neural morphogenesis, we derived neural tube organoids from WT and Par KO ESCs.

During the first two days of neural tube organoid induction, no significant morphological differences were observed between WT and Par KO organoids. By day 3, as ESCs transitioned toward an epiblast-like state, WT organoids developed columnar epithelial-like cells that radiated in an organized pattern from the central point. On day 4, nearly all WT organoids formed circular,

sharply defined luminal structures at their centers. These lumens progressively expanded and spontaneously elongated into oval shapes. By day 6, approximately 60% of WT organoids further developed into narrow, well-defined elliptical luminal structures (Fig. 6A-B).

In contrast, Par KO organoids failed to form columnar cellular structures and displayed disorganized cell alignment without radial symmetry on day 3. By day 4, these organoids exhibited only volume increase without forming typical lumens. By day 5, only a small fraction of Par KO organoids (~18%) formed lumen-like structures; however, these structures were small, circular, poorly delineated, and failed to elongate. By day 6, these aberrant lumens showed no further expansion or elongation (Fig. 6A-B).

During subsequent maturation culture (days 7–10), approximately 63% of WT neural tube organoids differentiated into numerous cells with neuronal axons. In contrast, Par KO organoids exhibited substantial apoptosis, with only about 13% developing axon-bearing cells (Fig. 6C-D). Immunofluorescence analysis for neural crest cell markers (SOX10), early neuron markers (TUJ1), and mature neuron markers (NeuN) revealed abundant neural crest cells and neurons in WT neural tube organoids, whereas Par KO organoids showed significantly reduced numbers of these cell types (Fig. 6E). These results demonstrate that loss of the Par complex severely disrupts the differentiation and maturation of ESCs into neural tube.

We next examined whether the morphogenetic defects in Par KO neural tube organoids could be rescued by co-culture with WT ESCs, WT CM, MK2206 or PF562271. All four treatments significantly enhanced both lumen formation efficiency and the frequency of spontaneous elongation by day 6 (Fig. 6F-G). Immunofluorescence analysis was performed to assess the localization of apical markers (ZO1, CD133) and the expression of NSC markers (PAX6, NESTIN). In untreated Par KO organoids, while PAX6 and NESTIN were expressed, ZO1 and CD133 showed aberrant localization with loss of apical polarity. All rescue treatments restored the apical distribution of ZO1 and CD133 to a pattern resembling that of WT organoids (Fig. 6H). During maturation culture, the four treatments, including co-culture with WT ESCs, WT CM, MK2206 or PF562271, can also promote the survival and maturation efficiency of Par KO organoids (Fig. 6I-J).

Collectively, these findings identify a critical role for the Par complex in maintaining apical-basal polarity and promoting lumenogenesis during neural tube morphogenesis. The successful rescue of these morphological defects, which achieved through co-culture with WT cells, WT CM, MK2206, or PF562271, confirms the functional centrality of the FAK signaling pathway downstream of Par complex activity.

Discussion

Cell polarity establishment marks a critical transition for embryos to initiate lineage specification, a process governed by conserved polarity complexes (Etemadmoghadam et al., 1995; Wang et al., 2018). Here, by generating Crumbs, Par, or Scrib complex knockout cells, we identified a specific and essential role for the Par complex during NPT. Par deficient cells failed to adopt the characteristic flat monolayer morphology of WT primed cells, highlighting its dominant function in morphological organization. This aligns with studies showing that targeted Par complex localization can induce polarity de novo (Watson et al., 2023). Further analysis revealed that Par loss disrupted apical junctional integrity, as evidenced by mislocalization of the adherens junction marker CDH1 and the tight junction marker ZO1. This supports the established role of the Par complex in forming and stabilizing both junction types (Hirose et al., 2002). Functionally, Par KO impaired differentiation across all three germ layers in EB and teratoma assays, and specifically disrupted NSC formation. The profound differentiation defect likely stems from the fundamental role of the Par complex in establishing polarity of various cell types during embryonic development, as exemplified by the finding that even a single amino acid mutation in *Par3* is sufficient to cause neural tube defects (Chen et al., 2017). Collectively, our results establish the Par complex as a master regulator of ESC differentiation potential, providing a mechanistic basis for the early embryonic lethality observed upon its deletion (Alarcon, 2010).

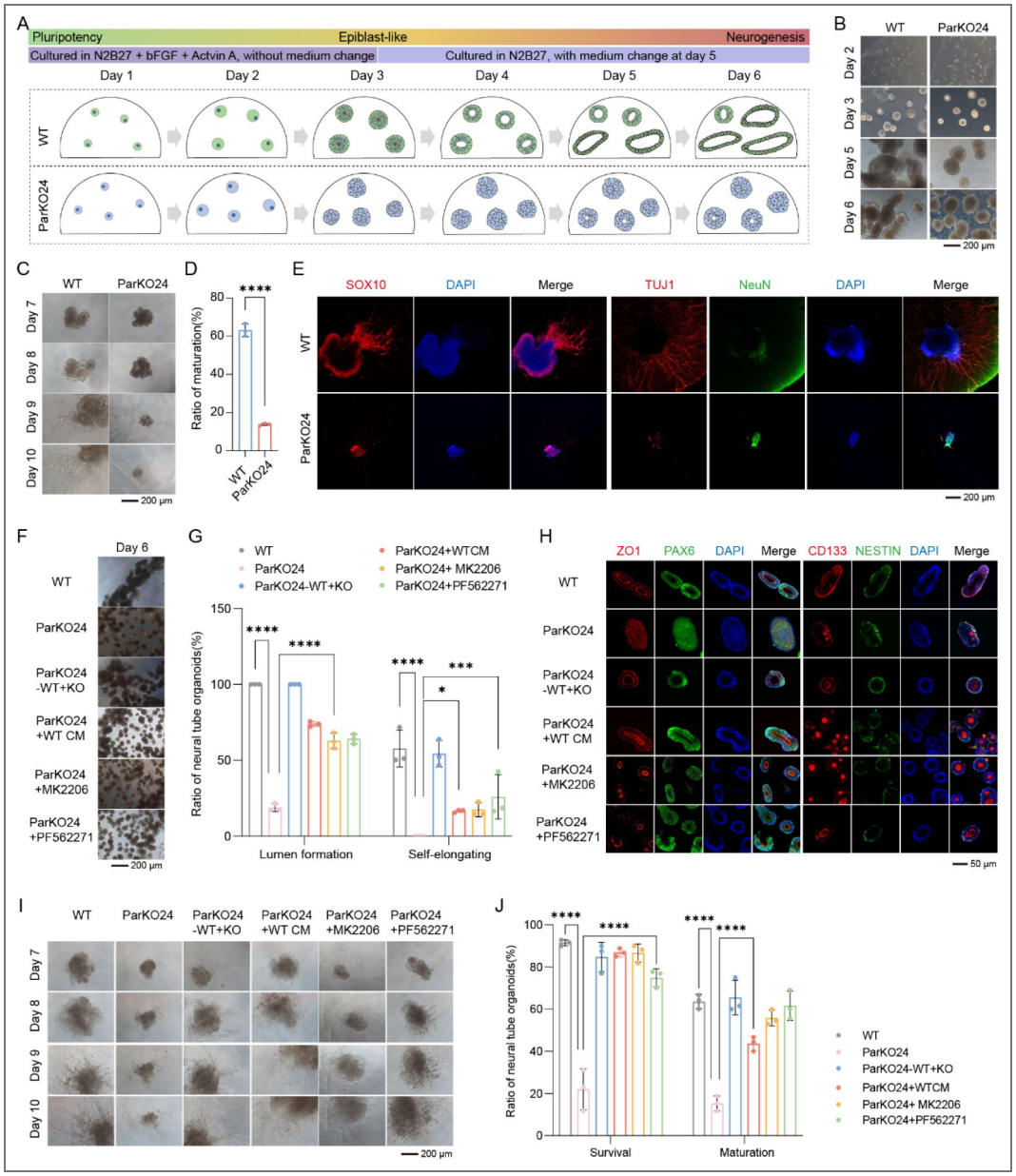

Figure 6. Par KO impairs neural tube organoids formation and maturation via the AKT–FAK signaling axis.

(A) Schematic illustration of neural tube organoid induction. **(B)** The morphological changes of WT and Par KO cells during neural tube organoids induction. **(C-D)** The neural tube organoids were subjected to subsequent maturation culture, the morphological differences were recorded **(C)** and maturation rate were analyzed **(D)**. **(E)** Mature neural tube organoids were assessed by immunofluorescence for markers of neural crest cells and neurons, such as SOX10, TUJ1, and NeuN. **(F-G)** Par KO ESCs were treated with co-culture, WT CM, MK2206, or PF562271 during neural tube organoid induction, the lumen formation and spontaneous elongation efficiency under different condition was assessed. **(H)** After treatment with co-culture, WT CM, MK2206, and PF562271, the expression of the lumen markers (ZO1 and CD133) as well as the NSC markers (PAX6 and NESTIN) was detected in Par KO neural tube organoids. **(I-J)** Par KO ESCs were treated with co-culture, WT CM, MK2206, or PF562271 during neural tube organoid maturation culture, the survival and maturation efficiency under different condition was assessed. Experiments were repeated for at least three times unless otherwise mentioned. Error bars represent S.D. One-way and two-way ANOVA analysis were performed in **(D)** and **(G, J)**, respectively.

The establishment of epithelial cell polarity critically depends on the ECM, a network primarily composed of collagen, laminin, and glycoproteins that regulates cell adhesion and provides spatial cues through integrin-mediated signaling (Sun et al., 2019). Our transcriptomic analysis revealed that Par KO disrupts this axis, with dysregulation of genes involved in ECM-receptor interaction, focal adhesion, and cytoskeleton organization during NPT. Both AKT and FAK inhibition rescued the flat monolayer morphology in Par KO primed cells. Notably, AKT inhibition reduced FAK phosphorylation, positioning FAK as a key downstream effector in maintaining cell morphology. This is consistent with the known ability of FAK to regulate cell adhesion and ECM-cell interaction (Dawson et al., 2021). This regulatory node was further highlighted by the rescue achieved with WT CM, which also normalized p-FAK levels (D Ilić, 1995). Proteomic analysis identified differential expression of proteins involved in cell adhesion and integrin signaling between WT and Par KO CM. Transcriptional profiling further revealed that genes commonly upregulated in MK2206-treated Par KO cells, WT CM-treated Par KO cells, and WT cells were enriched in pathways governing cell adhesion and ECM organization. Among the candidate factors, LEFTY1/2 stood out for their strong rescue capability and their higher abundance in WT CM versus Par KO CM, suggesting LEFTY acts as a critical extracellular mediator supplied by WT cells.

The functional importance of this pathway extends beyond morphology. Inhibition of FAK signaling restored the impaired differentiation potential of Par KO cells across multiple assays: EB differentiation, teratoma formation, and directed NSC differentiation. This demonstrates that Par complex governs differentiation capacity through a conserved, morphology-linked mechanism. (WT CM was omitted from EB differentiation assays due to volume constraints in the suspension culture system.) Notably, we observed a nuanced interaction in co-culture system: while WT cells rescued the morphological defects, they simultaneously suppressed proliferation of Par KO cells (Fig. 3D-E). This suggests the activation of cell competition, a quality-control process that may selectively eliminate suboptimal cells during development (Di Gregorio et al., 2016; Hashimoto & Sasaki, 2020; Maruyama & Fujita, 2022). Collectively, our findings delineate a signaling pathway in which the Par complex governs cell polarity establishment by sequentially modulating AKT activity, FURIN-mediated LEFTY maturation, ECM-integrin signaling, and ultimately FAK phosphorylation.

The Par complex plays a key regulatory role in apical-basal axis establishment during neural tube formation (AC et al., 2010; Zhang & Wei, 2022). In mice, *Pard3* deficiency causes neural developmental abnormalities and mid-gestational embryonic lethality (T et al., 2006). Recent studies have shown that Par complex abnormalities disrupt apical tight junctions and neuroepithelial polarization, contributing to NTDs in humans (Chen et al., 2017; Gao et al., 2012). Consistent with these findings, using ESC-derived neural tube organoids, we demonstrated that Par complex deficiency significantly reduces lumen structure formation efficiency and impairs spontaneous elongation. During maturation, Par KO neural tube organoids exhibited increased apoptosis and reduced maturation efficiency, underscoring the critical role of the Par complex in neural tube formation. Treatment with WT CM, MK2206, or PF562271 significantly improved lumen formation and maturation efficiency, with PF562271 showing the most prominent rescue effect. These results establish FAK phosphorylation as a critical downstream mediator of Par complex-regulated ESC differentiation and neural tube formation. This insight not only deepens our understanding of developmental plasticity but also suggests promising therapeutic strategies for NTDs.

Materials and Methods

Animal model

Female BALB/C Nude mice were purchased from GemPharmatech and maintained in ventilated cages under a 12:12 light:dark cycle at a controlled temperature, having *ad libitum* access to standard food and water. Five-week-old mice were used in this paper for the subcutaneous tumor formation assay, and maintained in the same conditions for 4 weeks. The experimental protocol

Key Resources Table				
Reagent type (species) or resource	**Designation**	**Source or reference**	**Identifiers**	**Additional information**
strain, strain background (*Escherichia coli*)	Stbl3 bacteria	Thermo Fisher Scientific	C737303	N/A
strain, strain background (*Escherichia coli*)	Lenti CRISPR v2	Addgene	#52961	Knockout vector
biological sample (include species here)	BALB/C Nude	GemPharmatech	Mouse strain: D000521	N/A
cell line (*M. musculus*)	OG2 mouse embryonic stem cells	Give from Dr. Duanqing Pei	N/A	Cell line maintained in Dr. Duanqing Pei lab.
cell line (*M. musculus*)	OG2-Crumbs KO ESC	This paper	N/A	Cell line maintained in Dr. Hui Zheng lab.

Key resources table.

cell line (*M. musculus*)	OG2-Par KO ESC	This paper	N/A	Cell line maintained in Dr. Hui Zheng lab.
cell line (*M. musculus*)	OG2-Scrib KO ESC	This paper	N/A	Cell line maintained in Dr. Hui Zheng lab.
cell line (*Homo-sapiens*)	293T	ATCC	CRL-3216	N/A
transfected construct (*M. musculus*)	Lenti CRISPR v2-Crb3	This paper	N/A	Lentiviral construct to transfect and express the sgRNA.
transfected construct (*M. musculus*)	Lenti CRISPR v2-Pals1	This paper	N/A	Lentiviral construct to transfect and express the sgRNA.
transfected construct (*M. musculus*)	Lenti CRISPR v2-Patj	This paper	N/A	Lentiviral construct to transfect and express the sgRNA.
transfected construct (*M. musculus*)	Lenti CRISPR v2-Mpdz	This paper	N/A	Lentiviral construct to transfect and express the sgRNA.
transfected construct (*M. musculus*)	Lenti CRISPR v2-Prkci	This paper	N/A	Lentiviral construct to transfect and express the sgRNA.
transfected construct (*M. musculus*)	Lenti CRISPR v2-Par3	This paper	N/A	Lentiviral construct to transfect and express the sgRNA.

Key resources table. (continued)

transfected construct (*M. musculus*)	Lenti CRISPR v2-Par6	This paper	N/A	Lentiviral construct to transfect and express the sgRNA.
transfected construct (*M. musculus*)	Lenti CRISPR v2-Scrib	This paper	N/A	Lentiviral construct to transfect and express the sgRNA.
transfected construct (*M. musculus*)	Lenti CRISPR v2-Llgl1	This paper	N/A	Lentiviral construct to transfect and express the sgRNA.
transfected construct (*M. musculus*)	Lenti CRISPR v2-Dlg1	This paper	N/A	Lentiviral construct to transfect and express the sgRNA.
antibody	Anti-CRB3 antibody [14F9]	Abcam	ab180835; RRID: AB_2890653	WB (1:1000)
antibody	Anti-PALS1(G-5) antibody	Santa Cruz Biotechnology	sc-365411; RRID: AB_10851475	WB (1:1000)
antibody	Anti-MUPP1 Polyclonal antibody (Anti-MPDZ)	Thermo Fisher Scientific	PA5-42259; RRID: AB_2610001	WB (1:1000)
antibody	Anti-PATJ antibody	Abcam	ab84932; RRID: AB_1925299	WB (1:1000)
antibody	Anti- Pals1 (G-5) Antibody	Santa Cruz Biotechnology	sc-365411; RRID: AB_10851475	WB (1:1000)

Key resources table. (continued)

antibody	Anti-PKC lambda/iota (H-12) antibody	Santa Cruz Biotechnology	sc-17837; RRID: AB_2172068	WB (1:1000)
antibody	Anti-PARD3 Polyclonal antibody	Thermo Fisher Scientific	PA5-106519; RRID: AB_2854188	WB (1:1000)
antibody	Anti-PARD6A (C-3) antibody	Santa Cruz Biotechnology	sc-365323; RRID: AB_10846183	WB (1:1000)
antibody	Anti-SCRIBBLE antibody	Abcam	ab154067	WB (1:1000)
antibody	Anti-LLGL1 + LLGL2 antibody [EPR18899]	Abcam	ab183021	WB (1:1000)
antibody	Anti-DLG1 antibody (SAP97 monoclonal antibody (RPI 197.4))	Enzo Life Sciences	ADI-VAM-PS005-D; RRID: AB_2039530	WB (1:1000)
antibody	Anti-NANOG antibody	Abcam	ab80892; RRID: AB_2150114	IF (1:300)
antibody	Anti-E-Cadherin (4A2) Mouse mAb	Cell Signaling Technology	14472; RRID: AB_2728770	IF (1:300)

Key resources table. (continued)

antibody	Anti-ZO1 Monoclonal antibody (ZO1-1A12)	Thermo Fisher Scientific	33-9100; RRID: AB_2533147	IF (1:200)
antibody	Anti-AKT antibody	Cell Signaling Technology	9272; RRID: AB_329827	WB (1:1000)
antibody	Anti-Phospho – AKT (Thr308) antibody	Cell Signaling Technology	9275; RRID: AB_329828	WB (1:1000)
antibody	Anti-Phospho – AKT (Ser473) antibody	Cell Signaling Technology	9271; RRID: AB_329825	WB (1:1000)
antibody	Anti-Phospho-FAK (Tyr397) Monoclonal antibody (141-9)	Thermo Fisher Scientific	44-625G; RRID: AB_2533702	IF (1:300)
antibody	Anti-LEFTY1+LEFTY2 antibody [JE38-88]	HUABIO	HA722177	WB (1:1000)
antibody	Anti-FURIN, Recombinant Rabbit Monoclonal antibody [JB35-53]	HUABIO	ET7107-37; RRID: AB_3070749	WB (1:1000)
antibody	Anti-NESTIN	BD Biosciences	611659; RRID: AB_399177	IF (1:300); FACS (1:300)

Key resources table. (continued)

antibody	Anti-SOX10 antibody	Selleck	F1143	IF (1:200)
antibody	Anti-AP-2α antibody (3B5)	Santa Cruz Biotechnology	sc-12726; RRID: AB_667767	IF (1:100)
antibody	Anti-Neurobal Class III β-Tubulin (TUJ1) antibody	Beyotime Biotechnology	AT809; RRID: AB_2893434	IF (1:200)
antibody	Anti-NeuN antibody (rabbit)	Merck	ABN78; RRID: AB_10807945	IF (1:100)
antibody	Anti-CD133 (Prominin-1) Monoclonal antibody (13A4)	Thermo Fisher Scientific	14-1331-82; RRID: AB_467471	IF (1:300)
antibody	Anti-PAX6 antibody	Abcam	ab195045; RRID: AB_2750924	IF (1:300)
antibody	Anti-beta ACTIN antibody (HRP Conjugated)	AMANI	AM-Actin-HRP	WB (1:1500)
antibody	Anti-Histone H3 (tri methyl K4) antibody - ChIP	Abcam	ab8580; RRID: AB_306649	WB (1:1000)
antibody	Anti-Tri-Methyl-Histone H3 (Lys27)	Cell Signaling Technology	9733; RRID: AB_2616029	WB (1:1000)

Key resources table. (continued)

	(C36B11) Rabit mAb			
antibody	Alexa Fluor® 647 Phalloidin	Cell Signaling Technology	8940	IF (1:500)
antibody	Goat anti-Mouse IgG(H+L) Cross-Adsorbed Secondary Antibody, Alexa Fluor 568	Thermo Fisher Scientific	A10037; RRID: AB_11180865	IF (1:500)
antibody	Donkey anti-Rabbit IgG (H+L) Highly Cross-Adsorbed Secondary Antibody, Alexa Fluor™ 568	Thermo Fisher Scientific	A10042; RRID: AB_2534017	IF (1:500)
antibody	Goat anti-Rat IgG (H+L) Cross-Adsorbed Secondary Antibody, Alexa Fluor 647	Thermo Fisher Scientific	A21247; RRID: AB_141778	IF (1:500)
antibody	Goat anti-Rabbit IgG (H+L) Cross-Adsorbed Secondary Antibody, Alexa Fluor™ 647	Thermo Fisher Scientific	A-21244; RRID: AB_2535812	IF (1:500)

Key resources table. (continued)

antibody	Goat anti-Mouse IgM (Heavy chain) Secondary Antibody, Alexa Fluor™ 647	Thermo Fisher Scientific	A-21238; RRID: AB_2535807	IF (1:500)
antibody	Goat anti-Mouse IgG(H+L) (peroxidase/ HRP conjugated)	AMANI	AM-MuHRP-0100	WB (1:2000)
antibody	Goat anti-Rabbit IgG(H+L) (peroxidase/ HRP conjugated)	AMANI	AM-RaHRP-0100	WB (1:2000)
sequence-based reagent	sgRNA for Crb3	This paper	N/A	5'-CCGGCTGG AGCCTAAC AGGT
sequence-based reagent	sgRNA for Pals1	This paper	N/A	5'-TGGCGATA AGAGGAAA CGGA
sequence-based reagent	sgRNA for Patj	This paper	N/A	5'-AGTTGGCT GAGCAATC TGAG
sequence-based reagent	sgRNA for Mpdz	This paper	N/A	5' -GAGCTCCT TAAACCTC CGTG
sequence-based reagent	sgRNA for Prkci	This paper	N/A	5' -CGGGTGA AAGCCTA CTACCG
sequence-based reagent	sgRNA for Par3	This paper	N/A	5' -TGAGGCT

Key resources table. (continued)

				GAAAACT TTCATG
sequence-based reagent	sgRNA for Par6	This paper	N/A	5' - CAGTCCCG ATAGCATC GTCG
sequence-based reagent	sgRNA for Scrib	This paper	N/A	5' - TGCCGGTT ACAACGC CAGAG
sequence-based reagent	sgRNA for Llgl1	This paper	N/A	5' - GGGAGCT ATTCACCT GACCA
sequence-based reagent	sgRNA for Dlg1	This paper	N/A	5' - CACCTATT AAAGCCT GAAAG
commercial assay or kit	VeZol Reagent	Vazyme	R411-02	N/A
chemical compound, drug	β-Mercaptoeth anol	Gibco	21985-023	N/A
chemical compound, drug	PD0325901	Selleck	S1036	N/A
chemical compound, drug	CHIR99021	Selleck	S1263	N/A
chemical compound, drug	XAV939	selleck	S1108	N/A
chemical compound, drug	Activin A	Topscience	TMPJ-01471	N/A
chemical compound, drug	b-FGF	PEPROTECH	100-18B-100	N/A

Key resources table. (continued)

chemical compound, drug	BOS318	Topscience	T9964	N/A
chemical compound, drug	SC79	Selleck	S7863	N/A
chemical compound, drug	IWR-1	Selleck	S7086	N/A
chemical compound, drug	Y27632	Selleck	S1049	N/A
chemical compound, drug	LDN193189	Selleck	S2618	N/A
chemical compound, drug	DAPT	Selleck	S2215	N/A
chemical compound, drug	Rapamycin	Selleck	S1039	N/A
chemical compound, drug	MK2206	Selleck	S1078	N/A
chemical compound, drug	LY294002	Selleck	S1105	N/A
chemical compound, drug	PF562271	Topscience	T2465	N/A
chemical compound, drug	IM-12	Selleck	S7566	N/A
chemical compound, drug	Verteporfin	Topscience	T3112	N/A
chemical compound, drug	PY60	Topscience	T9566	N/A

Key resources table. (continued)

chemical compound, drug	Asiaticoside	Topscience	T3025	N/A
chemical compound, drug	Puromycin	Gibco	A1113803	N/A
chemical compound, drug	PEI	SIGMA	919012	N/A
chemical compound, drug	Polybrene	SIGMA	TR-1003	N/A
software, algorithm	GraphPad Prism Version 8.0	GraghPad	https://www.graphpad.com	N/A
software, algorithm	ImageJ software Version 1.54f	National Institutes of Health	https://imagej.net/ij/download.html	N/A
software, algorithm	R version 4.5.0	R Core Team	https://www.R-project.org	N/A
software, algorithm	IGV_2.15.4	Robinson JT et al.	https://igv.org	N/A
software, algorithm	FlowJo	BD Biosciences	https://www.flowjo.com	N/A
software, algorithm	TissueFAXS Viewer 7.1	TissueGnostics	www.tissuegnostics	N/A
software, algorithm	ZEN 2012	Carl Zeiss Microscopy GmbH	https://www.zeiss.com.cn/microscopy	N/A
software, algorithm	SnapGene 4.1.8	Dotmatics	https://www.snapgene.com/	N/A
other	DAPI stain	Thermo Fisher Scientific	62248	IF (1:1000)

Key resources table. (continued)

complies with the requirements of animal welfare ethics, has been approved by the animal experimental ethics review in Guangzhou Medical University, and is permitted to be carried out, with the ethics review number N2025-25023.

Cell culture

OG2 embryonic stem cells (egfp reporter genes driven by the Oct4 promoter, GOF18ΔPE, CBA/CaJ X C57BL/6J) (Szabó et al., 2002) used in this study were recovered from liquid nitrogen, and cultured in mES medium (containing DMEM/F12, Neurobasal, 1% GlutaMAX, 1% NEAA, 1% Sodium Pyruvate, 0.5% N2 supplement, 1% B27 supplement, 0.1 mM β-Mercaptoethanol, 1000 units/mL LIF, 3 μM CHIR99021, and 1 μM PD0325901). During passage, ESCs were digested with Accutase at room temperature for 2 minutes, then terminated by DMEM/F12.

Primed cells were derived from NPT induction, and cultured in NPT medium (containing DMEM/F12, Neurobasal, 1% GlutaMAX, 1% NEAA, 0.5% N2 supplement, 1% B27 supplement, 0.1 mM β-Mercaptoethanol, 20 ng/mL bFGF, 20 ng/mL Activin A, 2 μM XAV939, and 3 μM CHIR99021). During passage, primed cells were digested with Accutase at room temperature for 3 minutes, then terminated by DMEM/F12. After centrifugating at 250 × *g* for 5 minutes, the cell clusters were resuspended in fresh NPT medium and gently shaken to spread them into small clumps without dispersing them into single cell. An appropriate amount of cell clusters was transferred to a petri dish and placed in an incubator.

293T cells were purchased from ATCC (*https://www.atcc.org*), and cultured in MEF medium (containing DMEM/High Glucose, 10% FBS, 1% GlutaMAX, and 1% NEAA). During passage, 293T cells were digested with 0.25% Trypsin-EDTA at 37 °C for 1 minute, then terminated by MEF medium.

All cell lines were cultured at 37 °C in a humidified incubator with 5% CO_2, and routinely tested to exclude mycoplasma contamination.

Construct knockout cell lines

Specific sgRNA sequences targeting the corresponding genes were designed and cloned into the lentiCRISPRv2 vector to construct recombinant knockout plasmids (Julia Joung, et al, 2017). The recombinant lentiviruses were produced using a PEI-mediated lentiviral packaging system, and the viral supernatants were collected to infect ESCs. Following two rounds of viral infection, the ESCs were subjected to Puromycin selection for 1 day to obtain stably infected cell populations. The surviving ESCs were digested into single-cell suspensions, and monoclonal cell lines were isolated using the 96-well plate limiting dilution method. After expansion of the monoclonal ESCs, genotype sequencing and western bloting were performed to identify and select positive clones with complete knockout of the target gene for subsequent experiments. All sgRNA sequences were listed in Key Resources Table.

Naïve-to-primed transition (NPT)

ESCs were digested into single cells with Accutase and seeded into gelatin-precoated culture dishes at a density of 10,000 cells/cm². They were cultured in mES medium until cell adhesion (approximately 12 hours), then mES medium was replaced with NPT medium for continuous induction over 6 days with fresh medium replaced daily. During the NPT process, the percentage of round morphology was quantified based on both the number and area of cell clusters. In the first two days of NPT, individual Par KO ESCs progressively developed into separated, flat cell clusters. By day 3, these flat clusters began to contract, aggregate, and form domed colonies. Thus, the percentage of round morphology was calculated as the number of domed colonies divided by the total number of cell clusters. However, from day 3 to day 6, when adjacent flat clusters merged into continuous sheets, the number of flat clusters was estimated based on area. Specifically, using half the average distance between adjacent domed colonies as the radius, a circular area was defined to represent the typical area of a single flat cluster. This circular reference was then used to partition the merged flat regions and estimate the count of individual flat clusters.

ESC-to-neural stem cell (NSC) differentiation

ESCs were digested into single cells with Accutase and seeded into Matrigel-precoated culture dishes at a density of 10,000 cells/cm².They were cultured in mES medium until cell adhesion (approximately 8 hours), then mES medium was replaced with NSC medium (containing DMEM/F12, 1% N2 supplement, 2% B27 supplement). NSC differentiation was continued for 7 consecutive days, with fresh NSC medium replaced daily during this period. Matrigel (CORNING, 356234) was diluted with DMEM/F12 at a 1:1 ratio.

ESC-to-embryoid body (EB) differentiation

ESCs were digested into single cells with Accutase and resuspended in mES-lif-2i medium (containing DMEM/High Glucose, 15% FBS (Gibco, 1099141C), 1% GlutaMAX, 1% NEAA, 1% Sodium Pyruvate, 0.1 mM β-Mercaptoethanol), then diluted to a density of 20,000 cells/mL. After mixing thoroughly, 2 mL of the cell suspension was vertically and evenly dropped onto the inner side of the 10 cm² culture dish lid using multichannel pipette with 20 µL/drop. Subsequently, 3 mL PBS was added to the 10 cm² culture dish, and the lid with cell droplets was gently and quickly placed back on the dish.The dish was transferred to an incubator for hanging drop culture for 3 days, with no medium change during this period. On Day 3, EBs were collected into a centrifuge tube using a Pasteur pipette and allowed to settle naturally for approximately 5 minutes until the EBs precipitated to the bottom of the tube. The EBs were then gently transferred to a T25 flask containing 8 mL fresh mES-lif-2i medium. The flask was then transferred to a horizontal shaker inside the humidified incubator and cultured continuously for another 6 days at 60 RPM, 37 °C, and 5% CO_2, with 1 mL of fresh mES-lif-2i medium supplemented daily.

Teratoma formation assay in immunodeficient mouse

A total of 1×10^6 ESCs were transferred to a 1.5 mL EP tube with 1 mL DPBS, centrifuged to remove the DPBS, and the tube was kept on ice for subsequent operations. The ESCs were immediately resuspended in 100 µL of a mixture of DMEM/F12 and Matrigel (CORNING, CLS356234) at a 1:1 ratio, then subcutaneously injected into the dorsal region of the hind limb of immunodeficient mice using an insulin syringe.The mice were maintained in ventilated cages under a 12:12 light:dark cycle at a controlled temperature, having *ad libitum* access to standard food and water. After 4 weeks, the teratoma tissues were harvested, then processed for sectioning and hematoxylin-eosin (HE) staining. HE-stained sections were imaged by using the TG Tissue FAXS Plus ST (TissueGnostics, Austria), and the scanned images were analysed using TissueFAXS Viewer software (version 7.1.6245.142).

ESC-to-neural tube organoid differentiation

The method of neural tube organoid induction was performed as previously reported (JiSoo Park, et al, 2022). The ESCs were digested into single cells with Accutase and resuspended in N2B27 medium (containing DMEM/F12, Neurobasal, 0.5% GlutaMAX, 1% NEAA, 1% Sodium Pyruvate, 0.5% N2 supplement, 1% B27 supplement, 0.1 mM β-Mercaptoethanol). A total of 1200 cells were transferred to a new EP tube with 300 µL of N2B27 and centrifuged at 250 × *g* for 5 minutes, then embedded in 10 µL of Matrigel (CORNING, CLS354248) to a final concentration of 1200 cells/10 µl drop of Matrigel. The 10 µL cell suspension was dropped into one well of a 24-well plate (Corning) containing 500 µL of Epi medium (N2B27 supplemented with 12 ng/mL bFGF and 20 ng/mL Activin A), and cultured for 3 days without medium change. On day 3, the Epi medium was replaced with 1 mL of N2B27 medium and cultured for another 2 days. On day 5, the medium was replaced with 1 mL of fresh N2B27 medium and cultured until day 6.For maturation of neural tube organoid, the neural tube organoids in Matrigel drop on day 6 were gently dissolved with 500 µL mixture of 3 mg/mL Collagenase IV and 25 U dispase (both dissolved in HBSS), then the released organoids were re-embedded in Matrigel at a concentration of 1 organoid/10 µL and dropped into each well of a 96-well plate with glass bottom. 100 µL of N2B27 medium was added to each well. The organoids were further cultured until day 10, with the medium changed daily.

Immunostaining and confocal microscopy

For cellular immunofluorescence staining, cells were fixed in 4% paraformaldehyde (PFA) at room temperature for 30 minutes, then blocked in QuickBlock™ Blocking Buffer for Immunol Staining (Beyotime Biotechnology, P0260) at 37 °C for 30 minutes. Subsequently, primary antibodies and secondary antibodies were incubated sequentially. Primary antibodies were diluted at 1:200 in QuickBlock™ Primary Antibody Dilution Buffer for Immunol Staining (Beyotime Biotechnology, P0262), and incubated on a shaker at 4°C overnight. Secondary antibodies were diluted at 1:500 in QuickBlock™ Secondary Antibody Dilution Buffer for Immunofluorescence ((Beyotime Biotechnology, P0265), and incubated on a shaker at room temperature for 1 hour (protect from light hereafter). The nuclei were counterstained with 4',6-diamidino-2-phenylindole (DAPI). Confocal images of cells were captured using the Zeiss LSM 800, and the scanned images were analysed using ZEN software [ZEN 2012 (blue edition)].

Flow cytometry analysis

Cells were harvested and fixed in 4% PFA, then added permeabilization and blocking solution to permeabilize and block at room temperature for 30 minutes. Permeabilization and blocking solution contained PBS, 0.1% Triton X-100 and 1% FBS. Incubated primary antibody at 4 °C for 2 hours and secondary antibody at room temperature in the dark for 45 minutes. Primary antibody and secondary antibody were diluted to 1:200 and 1:500, respectively. After staining, cells were resuspended at an appropriate volume of PBS according to the cell number. Filtered the cells through a 300-mesh filter and analyzed using the CytoFLEX (BECKMAN COULTER).

RNA-seq and RT-quantitative PCR (RT-qPCR)

Samples were collected as this study described and lysed in VeZol Reagent (Vazyme, R411-02) before being sent to sequencing company (Guangzhou HeQin Biotechnology Co., Ltd.) for RNA-seq. For qPCR, total RNA was extracted from samples using VeZol Reagent, and 1 μg of RNA were reversed to cDNA with HiScript IV All-in One Ultra RT SuperMix for qPCR (Vazyme, R433-01). Then the transcript levels of the genes were quantified using ChamQ Blue Universal SYBR qPCR Master Mix (Vazyme, Q312-03) on a CFX-96 Real-Time system (CFX96, Bio-Rad). Primers used in this study are listed in Key Resource Table.

Immunoblotting

Proteins were separated by SDS-PAGE gel and transferred to PVDF membranes. Following this, the membranes were blocked for 1 hour at room temperature using 5% non-fat milk in TBST. The membranes were then probed with the primary antibodies overnight at 4°C. Incubated the secondary antibodies for 1 hour at room temperature, then imaged with Immobilon Western Chemiluminescent HRP Substrate on Chemiluminescent/ Fluorescent/ Gel Imaging and Analysis System (ChampChemi610Plus, SINSAGE).

Quantification and statistical analysis

All statistical analyses were performed using GraphPad Prism 8. Independent replicates: $n \geq 3$.

Data are presented as means ± SD unless otherwise indicated. Statistical comparisons between multiple grounds were determined by One-way ANOVA or Two-way ANOVA, correct for multiple comparisons using statistical hypothesis testing with Tukey. while comparisons between two individual groups were conducted using Student's t-test, unless otherwise indicated.The statistical analysis criteria were: * $P < 0.05$, ** $P < 0.01$, *** $P < 0.001$, **** $P < 0.0001$.

Materials availability

All materials, reagents, and transgenic lines generated in this article are available upon request to the lead contact.

Further information and requests for resources and reagents should be directed to and will be fulfilled by the lead contact, Hui Zheng (zheng_hui@gibh.ac.cn).

Data availability

All raw data generated in this study have been deposited in the China National Center for Bioinformation/National Genomics Data Center under GSA: CRA032782 and OMIX: OMIX012794.

Supplementary figures

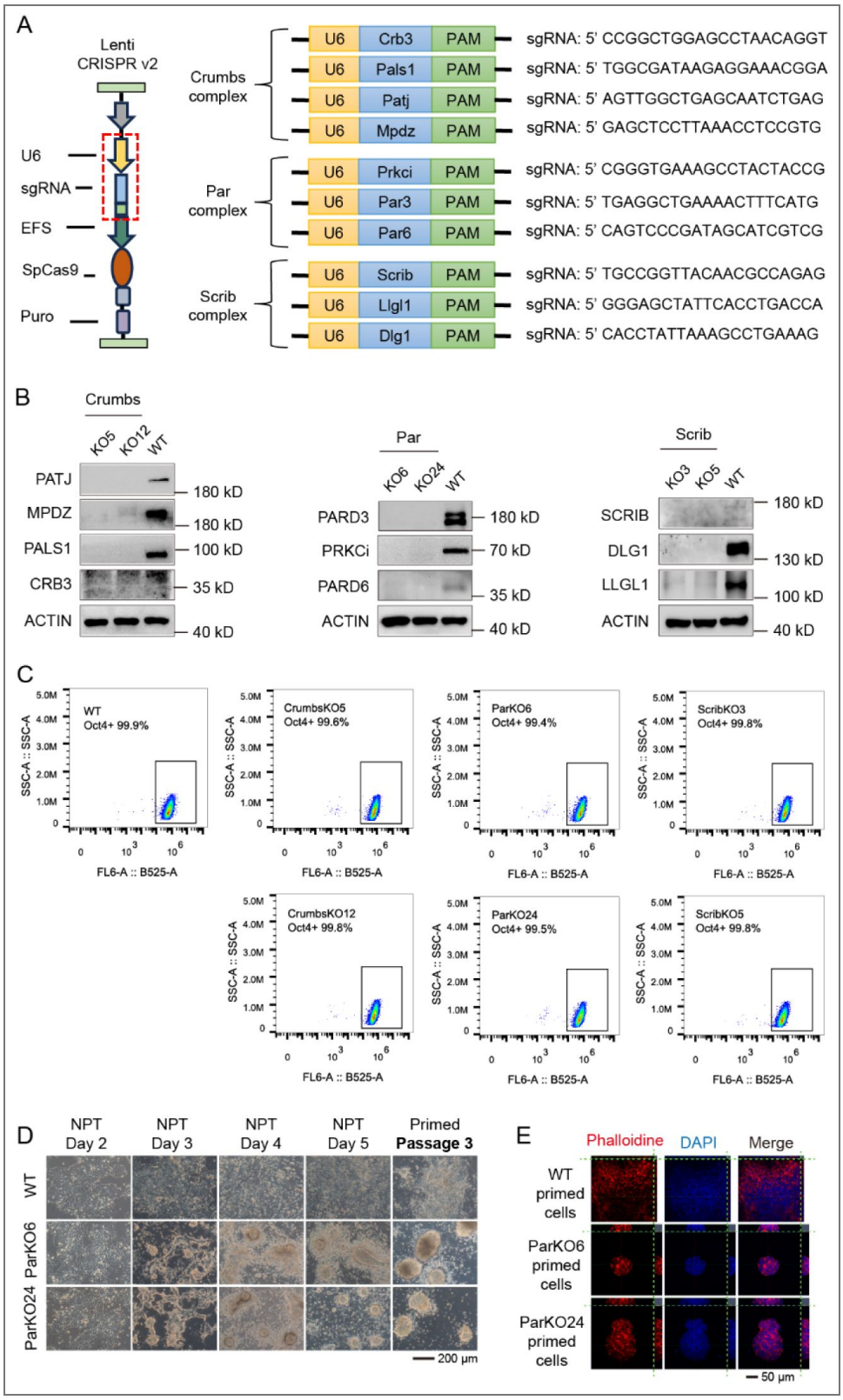

Supplemental Figure 1. Par complex is essential for NPT, related to Figure 1. (A) The sgRNA design strategy for knockout of Crumbs, Par, or Scrib complex. The plasmid was constructed using the CRISPR-cas9 technology. **(B)** Knockout efficiency for Crumbs, Par, and Scrib complexes was validated by WB. **(C)** Crumbs, Par, or Scrib complex KO did not affect ESCs pluripotency, the proportion of Oct4-GFP^{+} cells was not significantly different from

that of the WT. **(D)** Par complex KO caused the cells to exhibit a dome-shaped colony morphology, and this defect can be stably maintained at least three passages of culture. **(E)** WT primed cells presented flat monolayer clusters, while Par KO primed cells exhibited dome colonies, as visualized by Phalloidin staining and imaged by LSM800 confocal microscopy with Z-stack acquisition. Experiments were repeated for at least three times unless otherwise mentioned. Error bars represent S.D.

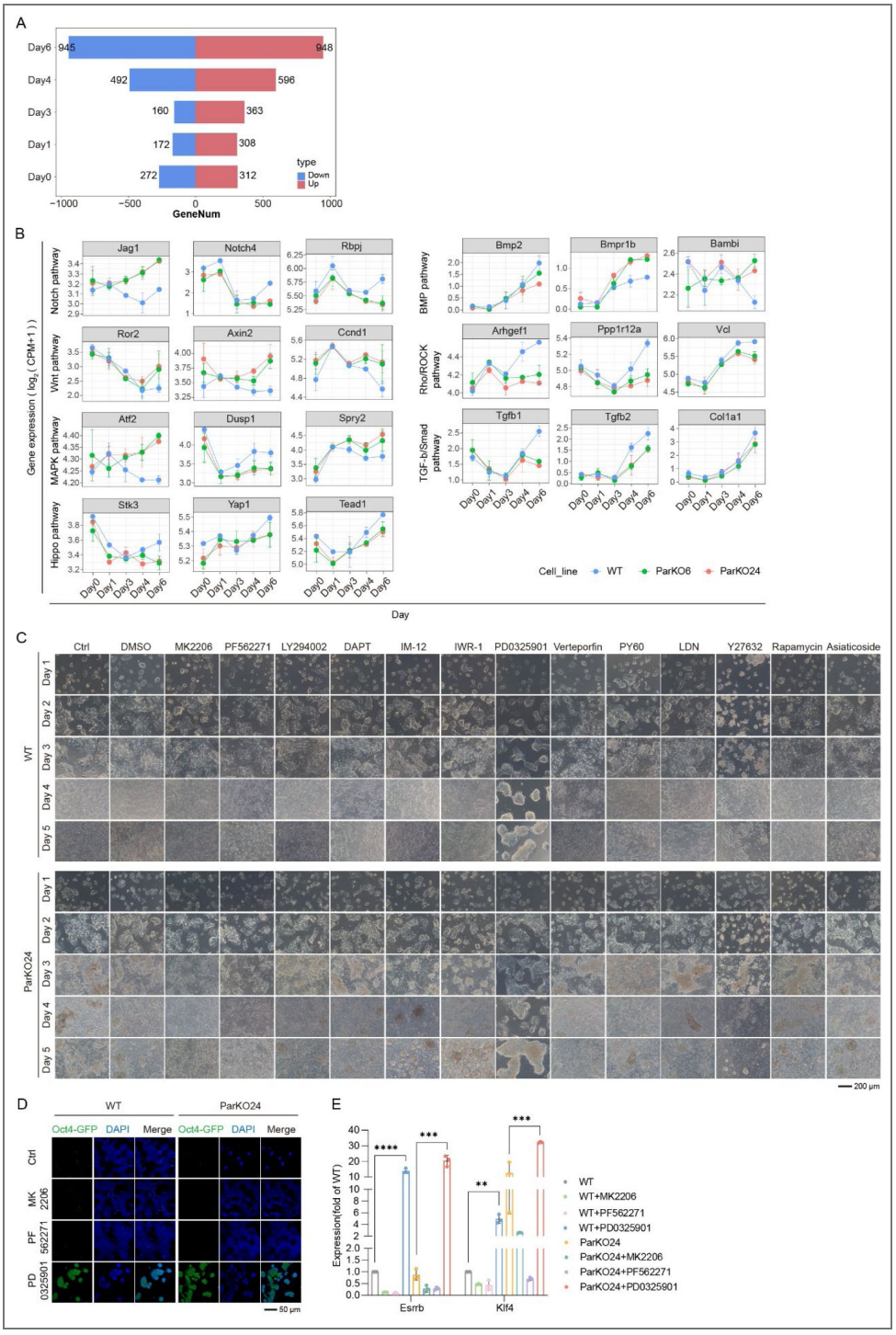

Supplemental Figure 2. AKT and FAK are key signal pathways that regulate cell morphology during NPT, related to Figure 2.

(A) The DEGs between Par KO and WT cells at different time points during NPT. The number of DEGs was the highest on Day 6. **(B)** Expression of key genes of the enriched pathways in (Figure 2D) was analyzed. **(C)** Cells were treated with agonists or inhibitors targeting the enriched pathways during NPT, followed by morphological analysis of dome colonies. **(D)** Par KO cells were treated with MK2206, PF562271, or PD0325901 during NPT and assessed Oct4-GFP^{+} expression. **(E)** The expression of ESC markers (such as *Esrrb* and *Klf4*) in cells treated with the MK2206, PF562271, and PD0325901 were analyzed during NPT. Experiments were repeated for at least three times unless otherwise mentioned. Error bars represent S.D. Two-way ANOVA analysis was performed in **(E)**.

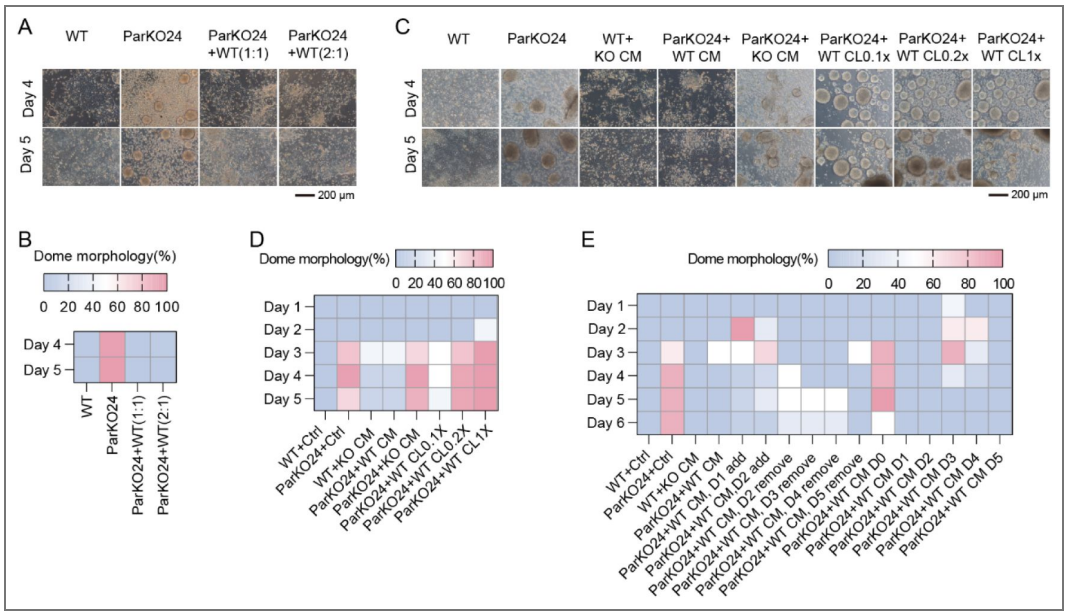

Supplemental Figure 3. **WT conditioned medium rescues the defect induced by Par KO, related to Figure 3.**

(A-B) NPT in co-culture system was carried out by mixing Par KO ESCs and WT ESCs at ratio of 1:1 or 2:1. Cell morphology was analyzed at the end of NPT. **(C-D)** Par KO ESCs were treated with WT CM, KO CM, or WT CL during NPT, and the cell morphology was analyzed. **(E)** The rescue effect of WT CM on Par KO ESCs showed a time-dependent pattern. WT CM must be present during the period from Day 2 to Day 4 of NPT to exert the rescue effect. While any collection of WT CM taken on Days 1 to Day 5 during NPT has a rescue effect. Experiments were repeated for at least three times unless otherwise mentioned. Error bars represent S.D.

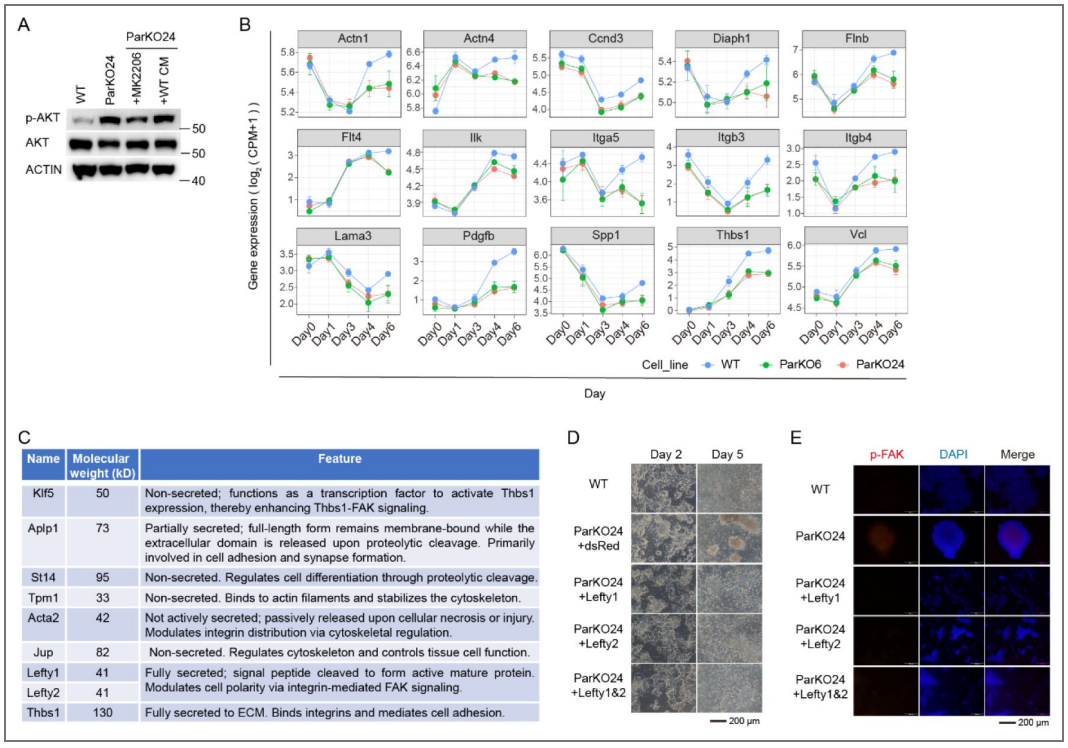

Supplemental Figure 4. Par complex mediates cell morphology through the AKT-FAK signal axis, related to Figure 4.

(A) Par KO cells were treated with MK2206, or WT CM during NPT, the p-AKT level were investigated on day 6. **(B)** Transcriptomic analysis of FAK-related DEGs between WT and Par KO cells during NPT using RNA-seq data. **(C)** Based on the FAK signaling pathway, functional candidate proteins were screened and subsequently overexpressed in Par KO ESCs to validate their biological roles. **(D)** Overexpression of LEFTY resulted in flat monolayer clusters of Par KO cells resembling that of the WT cells during NPT. **(E)** Overexpression of LEFTY in Par KO cells reduced the p-FAK level during NPT. Experiments were repeated for at least three times unless otherwise mentioned. Error bars represent S.D.

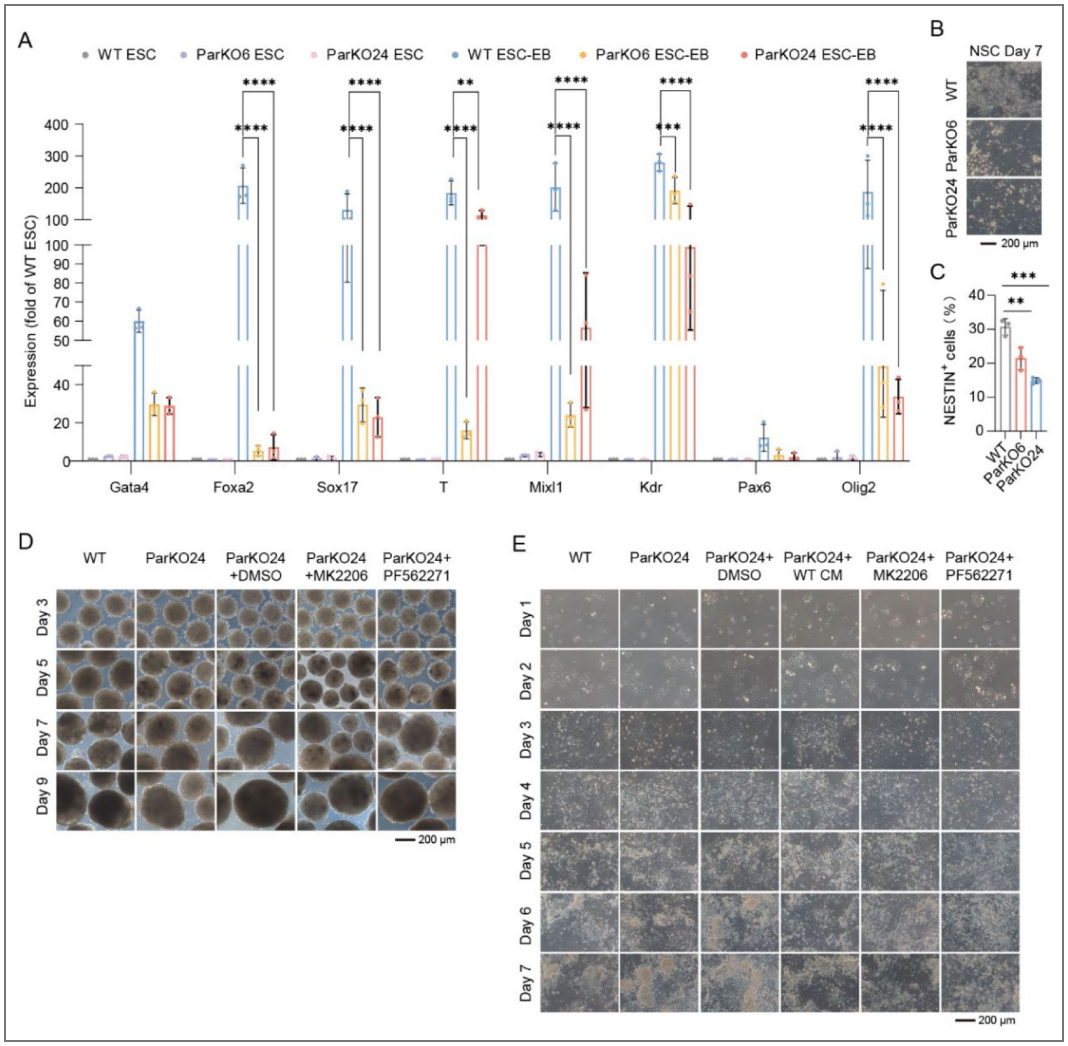

Supplemental Figure 5. Par KO impairs lineage differentiation via the AKT–FAK signaling axis, related to Figure 5.

(A) During EB differentiation from ESCs, expression of three germ layer markers was detected. **(B-C)** ESCs were induced to differentiate into NSCs. The cell morphology was analyzed, and the expression of NESTIN, a marker for NSCs, was detected. **(D)** Par KO ESCs were treated with MK2206 or PF562271 during the EB differentiation. The EB differentiation was performed using a suspension culture method. **(E)** Par KO ESCs were treated with MK2206 or PF562271 during the NSC differentiation. Experiments were repeated for at least three times unless otherwise mentioned. Error bars represent S.D. Two-way and one-way ANOVA analysis were performed in **(A)** and **(C)**, respectively.

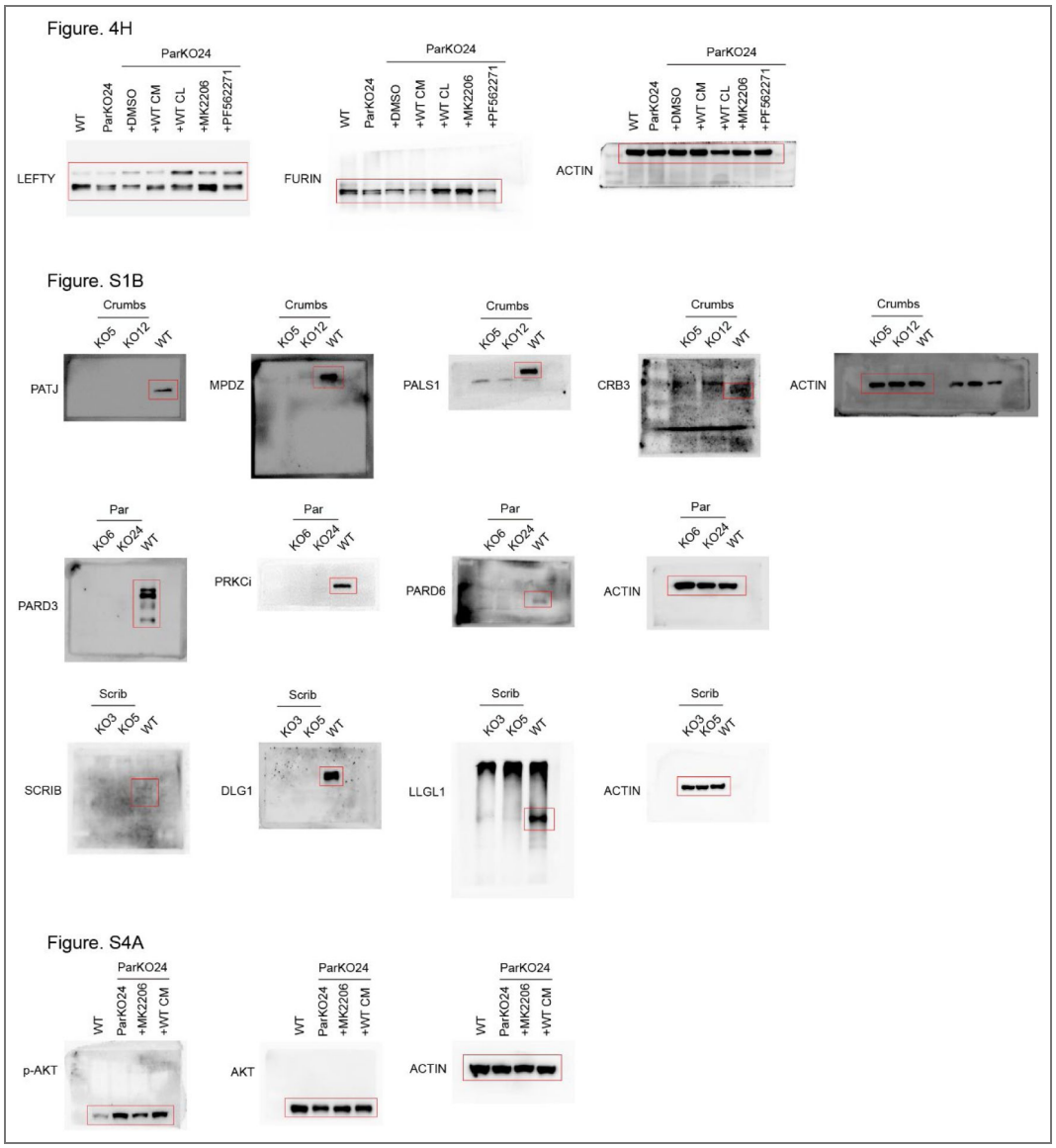

Supplemental Figure 6. **Uncropped gels, related to Figure 4, Figures S1 and S4.**

Additional information

Author contributions

Conceptualization, H.Z., L.N.L., D.J.Q.; Data Curation and Formal Analysis: M.A.H., Y.L.W., H.S., L.N.L.; Investigation: M.A.H., Y.Y.C., J.C.H., Y.H.W., Q.W.R., L.N.D., L.L., Q.Q.Z., T.Y.Z., X.Y.H., Q.G.; Supervision: H.Z., L.N.L., D.J.Q., L.G., C.P.L., S.Y.C.; Writing—Original Draft: M.A.H., L.N.L.; Writing—Review & Editing: M.A.H., L.N.L., H.Z.

Funding

Funder	Grant reference number	Author
MOST | National Key Research and Development Program of China (NKPs)	2024YFA1108201	Hui Zheng
MOST | National Key Research and Development Program of China (NKPs)	2024YFA1802303	Hao Sun
GDSTC | Basic and Applied Basic Research Foundation of Guangdong Province (廣東省基礎與應用基礎研究專項資金)	2024B1515040020	Hui Zheng
GDSTC | Basic and Applied Basic Research Foundation of Guangdong Province (廣東省基礎與應用基礎研究專項資金)	2024A1515010609	Lin Guo
Bureau of Science and Information Technology of Guangzhou Municipality | Guangzhou Municipal Science and Technology Project (Guangzhou Science and Technology Plan)	202201011654	Hao Sun
GDSTC | Science and Technology Planning Project of Guangdong Province (S&T Project of Guangdong Province)	2023B1212060050	Hui Zheng
GDSTC | Science and Technology Planning Project of Guangdong Province (S&T Project of Guangdong Province)	2023B1212120009	Hui Zheng
GDSTC | Guangdong Special Support Plan (广东省特殊支援计划)	2023TX07A051	Hui Zheng
中国博士后科学基金会职 | Postdoctoral Research Foundation of China (China Postdoctoral Research Foundation)	B202500701	Meiai He
Youth Innovation Promotion Association of the Chinese Academy of Sciences (CAS YIPA)	2022362	Lining Liang
Bureau of Education of Guangzhou Municipality	2024312185	Jingcai He
CAS | Guangzhou Institutes of Biomedicine and Health, Chinese Academy of Sciences (GIBH)	GIBHBRP23-01	Lin Guo
CAS | Guangzhou Institutes of Biomedicine and Health, Chinese Academy of Sciences (GIBH)	GIBHBRP24-01	Hui Zheng
CAS | Guangzhou Institutes of Biomedicine and Health, Chinese Academy of Sciences (GIBH)	GIBHBRP24-02	Hui Zheng
Research funds from Health @InnoHK Program		Hui Zheng

Author ORCID iDs

Hui Zheng: https://orcid.org/0000-0001-6801-0529

Additional files

Video 1. Related to Figure 1.

Video 2. Related to Figure 1.

Acknowledgements

The projects were supported by National Key R&D Program of China (2024YFA1108201 and 2024YFA1802303), Guangdong Basic and Applied Basic Research Foundation (2024B1515040020 and 2024A1515010609), Science and Technology Program of Guangzhou (202201011654), Science and Technology Planning Project of Guangdong Province (2023B1212060050 and 2023B1212120009), Guangdong Special Support Program (2023TX07A051), Postdoctoral Research Project Funding of He Meiai (B202500701), the Youth Innovation Promotion Association of the Chinese Academy of Sciences (2022362), the Tertiary Education Scientific research project of Guangzhou Municipal Education Bureau (2024312185), Basic Research Project of Guangzhou Institutes of Biomedicine and Health, Chinese Academy of Sciences (GIBHBRP23-01, GIBHBRP24-01, and GIBHBRP24-02), and Research Funds from Health @InnoHK Program launched by Innovation Technology Commission of the Hong Kong SAR, P. R. China.

References

Zovein AC, Luque A, Turlo KA, Hofmann JJ, Yee KM, Becker MS, Fassler R, Mellman I, Lane TF, Iruela-Arispe ML (2010) β1 Integrin Establishes Endothelial Cell Polarity and Arteriolar Lumen Formation via a Par3-Dependent Mechanism. *Dev Cell(1878-1551 (Electronic))* 39-51 https://doi.org/10.1016/j.devcel.2009.12.006 | PubMed

Adiyant Lamba M. Z., Meglicki Maciej, Czukiewska Sylwia, Balasubramaniam Lakshmi, Hadas Ron, Weishaupt Nina, Patel Ekta M, Kavanagh Yu Hua, Wang Ran, Jing Naihe, *et al.* (2025) Asynchronous mouse embryo polarization leads to heterogeneity in cell fate specification. *eLife* **8**:RP101140 https://doi.org/10.7554/eLife.101140 | PubMed

Alarcon V. B (2010) Cell polarity regulator PARD6B is essential for trophectoderm formation in the preimplantation mouse embryo. *Biol Reprod* **83**:347-358 https://doi.org/10.1095/biolreprod.110.084400 | PubMed

Alowayed N., Salker M. S., Zeng N., Singh Y., Lang F (2016) LEFTY2 Controls Migration of Human Endometrial Cancer Cells via Focal Adhesion Kinase Activity (FAK) and miRNA-200a. *Cellular Physiology and Biochemistry* **39**:815-826 https://doi.org/10.1159/000447792 | PubMed

Brons IG, Smithers LE, Trotter MW, Rugg-Gunn P, Sun B, Chuva de Sousa Lopes SM, Howlett SK, Clarkson A, Ahrlund-Richter L, Pedersen RA, *et al.* (2007) Derivation of pluripotent epiblast stem cells from mammalian embryos. *Nature* **448**:191-195 https://doi.org/10.1038/nature05950 | PubMed

Chen X., An Y., Gao Y., Guo L., Rui L., Xie H., Sun M., Lam Hung S., Sheng X., Zou J., *et al.* (2017) Rare Deleterious PARD3 Variants in the aPKC-Binding Region are Implicated in the Pathogenesis of Human Cranial Neural Tube Defects Via Disrupting Apical Tight Junction Formation. *Hum Mutat* **38**:378-389 https://doi.org/10.1002/humu.23153 | PubMed

D Ilić Y. F., Kanazawa S, Takeda N, Sobue K, Nakatsuji N, Nomura S, Fujimoto J, Okada M, Yamamoto T (1995) Reduced cell motility and enhanced focal adhesion contact formation in cells from FAK-deficient mice. *Nature* **377**:539-544 https://doi.org/10.1038/377539a0 | PubMed

Dawson J. C., Serrels A., Stupack D. G., Schlaepfer D. D., Frame M. C (2021) Targeting FAK in anticancer combination therapies. *Nature Reviews Cancer* **21**:313-324 https://doi.org/10.1038/s41568-021-00340-6 | PubMed

Di Gregorio A., Bowling S., Rodriguez Tristan A. (2016) Cell Competition and Its Role in the Regulation of Cell Fitness from Development to Cancer. *Developmental Cell* **38**:621-634 https://doi.org/10.1016/j.devcel.2016.08.012 | PubMed

Dias Gomes M., Iden S. (2021) Orchestration of tissue-scale mechanics and fate decisions by polarity signalling. *EMBO J* **40**:e106787 https://doi.org/10.15252/embj.2020106787 | PubMed

Diaz-Palacios K., López Navajas P., Rodrigo Martín B., Matesanz R., Luque-Ortega J. R., Echarri A., Lietha D (2025) Phospho-regulated tethering of focal adhesion kinase to vinculin links force transduction to focal adhesion signaling. *Cell Communication and Signaling* **23** https://doi.org/10.1186/s12964-025-02201-3 | PubMed

Dubois C. M., Blanchette F., Laprise M.-H., Leduc R., Grondin F., Seidah N. G (2001) Evidence that Furin Is an Authentic Transforming Growth Factor-β1-Converting Enzyme. *The American Journal of Pathology* **158**:305-316 https://doi.org/10.1016/s0002-9440(10)63970-3 | PubMed

Etemadmoghadam B., Guo S., Kemphues K. J (1995) Asymmetrically distributed PAR-3 protein contributes to cell polarity and spindle alignment in early C. elegans embryos. *Cell* **83**:743-752 https://doi.org/10.1016/0092-8674(95)90187-6 | PubMed

Fleming T. P., McConnell J., Johnson M. H., Stevenson B. R (1989) Development of tight junctions de novo in the mouse early embryo: control of assembly of the tight junction-specific protein, ZO-1. *J Cell Biol* **108**:1407-1418 https://doi.org/10.1083/jcb.108.4.1407 | PubMed

Gao Y., Chen X., Shangguan S., Bao Y., Lu X., Zou J., Guo J., Dai Y., Zhang T (2012) Association study of PARD3 gene polymorphisms with neural tube defects in a Chinese Han population. *Reprod Sci* **19**:764-771 https://doi.org/10.1177/1933719111433886 | PubMed

Guzman-Herrera A., Mao Y (2020) Polarity during tissue repair, a multiscale problem. *Curr Opin Cell Biol* **62**:31-36 https://doi.org/10.1016/j.ceb.2019.07.015 | PubMed

Hashimoto M., Sasaki H (2020) Cell competition controls differentiation in mouse embryos and stem cells. *Current Opinion in Cell Biology* **67**:1-8 https://doi.org/10.1016/j.ceb.2020.07.001 | PubMed

Hayashi K., Saitou M (2013) Stepwise differentiation from naive state pluripotent stem cells to functional primordial germ cells through an epiblast-like state. *Methods Mol Biol* **1074**:175-183 https://doi.org/10.1007/978-1-62703-628-3_13 | PubMed

Herrera A., Menendez A., Torroba B., Ochoa A., Pons S (2021) Dbnl and β-catenin promote pro-N-cadherin processing to maintain apico-basal polarity. *Journal of Cell Biology* **220** https://doi.org/10.1083/jcb.202007055 | PubMed

Hirose T., Izumi Y., Nagashima Y., Tamai-Nagai Y., Kurihara H., Sakai T., Suzuki Y., Yamanaka T., Suzuki A., Mizuno K., *et al.* (2002) Involvement of ASIP/PAR-3 in the promotion of epithelial tight junction formation. *Journal of Cell Science* **115**:2485-2495 https://doi.org/10.1242/jcs.115.12.2485 | PubMed

Hong E., Jayachandran P., Brewster R (2010) The polarity protein Pard3 is required for centrosome positioning during neurulation. *Dev Biol* **341**:335-345 https://doi.org/10.1016/j.ydbio.2010.01.034 | PubMed

Ivachtchenko A. V., Khvat A. V., Shkil D. O (2024) Development and Prospects of Furin Inhibitors for Therapeutic Applications. *International Journal of Molecular Sciences* **25** https://doi.org/10.3390/ijms25179199 | PubMed

Kalkan T., Olova N., Roode M., Mulas C., Lee H. J., Nett I., Marks H., Walker R., Stunnenberg H. G., Lilley K. S., *et al.* (2017) Tracking the embryonic stem cell transition from ground state pluripotency. *Development* **144**:1221-1234 https://doi.org/10.1242/dev.142711 | PubMed

Korotkevich E., Niwayama R., Courtois A., Friese S., Berger N., Buchholz F., Hiiragi T (2017) The Apical Domain Is Required and Sufficient for the First Lineage Segregation in the Mouse Embryo. *Dev Cell* **40**:235-247.e237. https://doi.org/10.1016/j.devcel.2017.01.006 | PubMed

Legere E.-A., Baumholtz A. I., Lachance J.-F. B., Archer M., Piontek J., Ryan A. K (2024) Claudin-3 in the non-neural ectoderm is essential for neural fold fusion in chicken embryos. *Developmental Biology* **507**:20-33 https://doi.org/10.1016/j.ydbio.2023.12.009 | PubMed

Leung C. Y., Zhu M., Zernicka-Goetz M (2016) Polarity in Cell-Fate Acquisition in the Early Mouse Embryo. *Curr Top Dev Biol* **120**:203-234 https://doi.org/10.1016/bs.ctdb.2016.04.008 | PubMed

Li X., Combs J. D., Salaita K., Shu X (2023) Polarized focal adhesion kinase activity within a focal adhesion during cell migration. *Nature Chemical Biology* **19**:1458-1468 https://doi.org/10.1038/s41589-023-01353-y | PubMed

MacGowan J., Cardenas M., Williams M. K (2025) Fold-and-fuse neurulation in zebrafish requires vangl2. *Developmental Biology* **524**:55-68 https://doi.org/10.1016/j.ydbio.2025.05.001 | PubMed

Maruyama T., Fujita Y (2022) Cell competition in vertebrates — a key machinery for tissue homeostasis. *Current Opinion in Genetics & Development* **72**:15-21 https://doi.org/10.1016/j.gde.2021.09.006 | PubMed

Meng Zhu M. S., Martin Angel, et al. (2021) Human embryo polarization requires PLC signaling to mediate trophectoderm specification. *eLife* **27**:e65068 https://doi.org/10.7554/eLife.65068 | PubMed

Nelson W. J (2003) Adaptation of core mechanisms to generate cell polarity. *Nature* **422**:766-774 https://doi.org/10.1038/nature01602 | PubMed

Nychyk O., Galea G. L., Molè M., Savery D., Greene N. D. E., Stanier P., Copp A. J (2022) Vangl2–environment interaction causes severe neural tube defects, without abnormal neuroepithelial convergent extension. *Disease Models & Mechanisms* **15** https://doi.org/10.1242/dmm.049194 | PubMed

Rostovskaya M., Stirparo G. G., Smith A (2019) Capacitation of human naive pluripotent stem cells for multi-lineage differentiation. *Development* **146** https://doi.org/10.1242/dev.172916 | PubMed

Sakthivel K., Kotowska A., Fan Z., Portner E. J., Merry C., Nordenfelt P., Simonsen A. C., Wright A. J., Swaminathan V. S (2025) Integrin-Piezo1 Axis Drives ECM Remodeling and Invasion of 3D Breast Epithelium. *Advanced Science* https://doi.org/10.1002/advs.202509932 | PubMed

Shi D.-L (2022) Wnt/planar cell polarity signaling controls morphogenetic movements of gastrulation and neural tube closure. *Cellular and Molecular Life Sciences* **79** https://doi.org/10.1007/s00018-022-04620-8 | PubMed

Sun Z., Costell M., Fassler R (2019) Integrin activation by talin, kindlin and mechanical forces. *Nat Cell Biol* **21**:25-31 https://doi.org/10.1038/s41556-018-0234-9 | PubMed

Hirose T, Karasawa M, Sugitani Y, Fujisawa M, Akimoto K, Ohno S, Noda T (2006) PAR3 is essential for cyst-mediated epicardial development by establishing apical. *Development* 1389-1398 https://doi.org/10.1242/dev.02294 | PubMed

Tesar P. J., Chenoweth J. G., Brook F. A., Davies T. J., Evans E. P., Mack D. L., Gardner R. L., McKay R. D (2007) New cell lines from mouse epiblast share defining features with human embryonic stem cells. *Nature* **448**:196-199 https://doi.org/10.1038/nature05972 | PubMed

Tokamov S. A., Nouri N., Rich A., Buiter S., Glotzer M., Fehon R. G (2023) Apical polarity and actomyosin dynamics control Kibra subcellular localization and function in Drosophila Hippo signaling. *Developmental Cell* **58**:1864-1879.e1864. https://doi.org/10.1016/j.devcel.2023.08.029 | PubMed

Wang J., An Z., Wu Z., Zhou W., Sun P., Wu P., Dang S., Xue R., Bai X., Du Y., *et al.* (2024) Spatial organization of PI3K-PI(3,4,5)P3-AKT signaling by focal adhesions. *Molecular Cell* **84**:4401-4418.e4409. https://doi.org/10.1016/j.molcel.2024.10.010 | PubMed

Wang X., Dong B., Zhang K., Ji Z., Cheng C., Zhao H., Sheng Y., Li X., Fan L., Xue W., *et al.* (2018) E-cadherin bridges cell polarity and spindle orientation to ensure prostate epithelial integrity and prevent carcinogenesis in vivo. *PLoS Genet* **14**:e1007609 https://doi.org/10.1371/journal.pgen.1007609 | PubMed

Wang Y., Shen N., Yang Y., Xia Y., Zhang W., Lu Y., Wang Z., Yang Z., Wang Z (2024) ZDHHC5-mediated S-palmitoylation of FAK promotes its membrane localization and epithelial-mesenchymal transition in glioma. *Cell Communication and Signaling* **22** https://doi.org/10.1186/s12964-023-01366-z | PubMed

Watson J. L., Kruger L. K., Ben-Sasson A. J., Bittleston A., Shahbazi M. N., Planelles-Herrero V. J., Chambers J. E., Manton J. D., Baker D., Derivery E (2023) Synthetic Par polarity induces cytoskeleton asymmetry in unpolarized mammalian cells. *Cell* **186**:4710-4727.e4735. https://doi.org/10.1016/j.cell.2023.08.034 | PubMed

Weinberger L., Ayyash M., Novershtern N., Hanna J. H (2016) Dynamic stem cell states: naive to primed pluripotency in rodents and humans. *Nat Rev Mol Cell Biol* **17**:155-169 https://doi.org/10.1038/nrm.2015.28 | PubMed

Xu S., Pang L., Liu Y., Lian X., Mo K., Lv R., Zhu H., Lv C., Lin J., Sun J., *et al.* (2019) Akt plays indispensable roles during the first cell lineage differentiation of mouse. *J Mol Histol* **50**:369-374 https://doi.org/10.1007/s10735-019-09833-z | PubMed

Ying Q.-L., Wray J., Nichols J., Batlle-Morera L., Doble B., Woodgett J., Cohen P., Smith A (2008) The ground state of embryonic stem cell self-renewal. *Nature* **453**:519-523 https://doi.org/10.1038/nature06968 | PubMed

Yonemura S I. M., Nagafuchi A, Tsukita S (1995) Cell-to-cell adherens junction formation and actin filament organization. *Journal of cell science* **108**:127-142 https://doi.org/10.1242/jcs.108.1.127 | PubMed

Zhan L., Rosenberg A., Bergami K. C., Yu M., Xuan Z., Jaffe A. B., Allred C., Muthuswamy S. K (2008) Deregulation of scribble promotes mammary tumorigenesis and reveals a role for cell polarity in carcinoma. *Cell* **135**:865-878 https://doi.org/10.1016/j.cell.2008.09.045 | PubMed

Zhang L., Wei X (2022) The Roles of Par3, Par6, and aPKC Polarity Proteins in Normal Neurodevelopment and in Neurodegenerative and Neuropsychiatric Disorders. *J Neurosci* **42**:4774-4793 https://doi.org/10.1523/jneurosci.0059-22.2022 | PubMed

Zhu M., Zernicka-Goetz M (2020) Building an apical domain in the early mouse embryo: Lessons, challenges and perspectives. *Curr Opin Cell Biol* **62**:144-149 https://doi.org/10.1016/j.ceb.2019.11.005 | PubMed

Meiai He (2025) Research on the establishment of cell polarity. China National Center for Bioinformation/National Genomics Data Center, GSA. ID CRA032782 https://ngdc.cncb.ac.cn/gsa/s/0Gc6v9ep

Meiai He (2025) Research on the establishment of cell polarity. China National Center for Bioinformation/National Genomics Data Center, OMIX. ID OMIX012794 https://ngdc.cncb.ac.cn/omix/preview/Mp2F7olK

Peer reviews

Reviewer #1 (Public review):

The study by He and colleagues aims to investigate the molecular mechanisms driving key cell potency transitions, particularly the naïve-to-primed pluripotency transition. The authors explore the relationship between cell polarity and stemness using stem cell models combined with a comprehensive panel of experiments, including pharmacological inhibition and co-culture/conditioned medium rescue approaches. Overall, the study provides interesting observations and contributes to the understanding of the molecular mechanisms dynamically regulating stem cell differentiation.

However, several conceptual and interpretational aspects could be strengthened:

First, the Introduction would benefit from being more focused on what is currently known regarding cell polarity during early embryogenesis and pluripotent stem cell transitions, rather than emphasizing later neurogenesis events. Such reorientation would better match the main topic of the manuscript and improve the conceptual coherence of the study.

Similarly, Figure 6, where the authors attempt to provide clinical relevance through neural organoid formation experiments, feels somewhat disconnected from the central theme of the naïve-to-primed transition. Although this section is interesting on its own, there is already extensive literature describing polarization and morphogenetic events occurring much earlier during pluripotent state transitions. Therefore, the developmental relevance of the neural differentiation phenotypes could be better contextualized in relation to earlier morphogenetic events associated with pluripotency progression.

The manuscript contains a substantial amount of experimental work; however, several results would benefit from deeper discussion. For example, in Figure 1, what is the rationale behind ZO1 downregulation being observed specifically in primed PAR knockout cells but not under naïve culture conditions? In addition, in Figure 3, the authors perform co-culture and conditioned medium experiments between wild-type and knockout cells. While the authors focus on the secreted protein fraction that rescues the phenotype, they also mention that other fractions display rescuing activity. Could the authors briefly discuss what additional components may contribute to this rescue effect? For example, could other molecules within these fractions also converge on AKT signaling regulation?

Importantly, transitions in cell potency are frequently associated with coordinated morphogenetic changes. For example, during mouse embryogenesis, naïve pluripotent inner cell mass cells progressively polarize into a rosette-like structure with apical domain specification before lumen formation and epithelialization during progression toward the primed epiblast state. This developmental context could help strengthen the biological interpretation of the study.

There are also several claims throughout the manuscript that appear to be overinterpreted or insufficiently quantified. For example, in Figure 1, the authors state that CDH1 expression is uniform; however, this is difficult to appreciate from the images shown, and quantitative analysis would be necessary to support this conclusion.

Another example appears in Figure 2, where the authors claim that "heatmap analysis revealed that transcriptomic profiles of PAR knockout cells progressively diverged from wild type from day 3 onwards". This conclusion is not fully supported by the presented data for two reasons: (1) transcriptomic divergence is more appropriately assessed through principal component analysis, clustering, or distance-based methods rather than by visual inspection of a heatmap alone; and (2) although some genes displayed in panel E begin to show genotype-associated differences from day 3, the overall transcriptomic structure shown in the PCA and heatmap remains primarily dominated by temporal progression rather than genotype.

In this context, it remains unclear whether PAR knockout cells truly retain a more naïve pluripotent transcriptomic identity. To support this claim, the authors should compare the knockout transcriptome directly against a naïve pluripotent population. The phenotype observed in the knockout cells may instead represent an incomplete or aberrant primed transition rather than maintenance of naïve pluripotency itself. Intermediate morphogenetic states, such as rosette-like epithelial stages, could also explain the observed phenotype.

Strengthening this aspect of the study would substantially improve its developmental and in vivo relevance, which currently appears somewhat limited. In particular, it would be interesting to determine whether this mechanism operates during embryogenesis itself. The authors could consider relatively simple but informative experiments, such as perturbing PAR signaling or Furin activity during embryo culture.

Along the same lines, some statements in the manuscript appear overly speculative. For example, the statement that "these findings may reveal a developmental compensation mechanism during embryogenesis, whereby normal cells rescue defective cells or increase

their own proportion" extends well beyond the experimental evidence presented. Such claims invoke concepts related to cell competition, abnormal cell recognition, or developmental quality control mechanisms in vivo, none of which are directly demonstrated in this study. The authors are encouraged either to substantially tone down these statements or move them to the Discussion as speculative possibilities.

Another important conceptual point concerns the relationship between PAR complex regulation and Lefty signaling. If this mechanism indeed reflects a physiological or homeostatic process operating during embryogenesis, what would be the developmental rationale for the PAR complex regulation of Lefty? Lefty is well known for its role during gastrulation and anterior epiblast patterning. It would therefore be interesting if the authors could further discuss potential links between these developmental contexts.

Minor points:

(1) The authors state that PAR knockout cells do not exhibit major differences in self-renewal capacity; however, they simultaneously claim that these cells remain in a more naïve-like state. This interpretation requires clarification, as naïve pluripotent cells are typically associated with increased clonogenicity, enhanced self-renewal, and expression of markers such as alkaline phosphatase and SSEA1 compared to primed cells. The relationship between the observed phenotype and the proposed "naïve-like" state should therefore be discussed more carefully.

(2) The authors generated several independent knockout clones, but appear to use only one clone for downstream analyses after observing similar morphogenetic phenotypes. Is this sufficient to account for potential clonal heterogeneity? Would the use of pooled clones provide a more robust experimental system?

(3) The rescue experiments using pathway inhibitors are interesting; however, the interpretation again relies primarily on colony morphology. Readers may question whether these experiments truly represent rescue of the naïve-to-primed transition itself without additional transcriptomic or molecular characterization.

(4) In Figure 4, the manuscript could be strengthened by integrating transcriptomic analyses from pharmacological treatments with the secreted-factor and co-culture datasets.

(5) The authors could better clarify the context of Furin downregulation in the knockout cells. Is this a direct consequence of altered transcriptional regulation by the PAR complex, or could it instead represent a secondary consequence of impaired progression through the primed pluripotent transition?

https://doi.org/10.7554/eLife.111448.1.sa2

Reviewer #2 (Public review):

Summary:

The study demonstrated that Par, but not other polarity genes, Crumbs or Scrib, regulates cell polarity during PSC transition to primed state as well as neural tube formation.

Strengths:

The use of KO convinces the role of Par in NPT. Scrib and Crumbs KO data are informative to the field. The conditioned medium experiment is informative. They suggested the potential secreted factors over 50kDa are responsible for maintaining the polarity of NPT in Par KO.

Weaknesses:

Most importantly, how Par is important for PSC maintenance and differentiation is not clear. The data provided are dome shape formation, endoderm lineage tendency, and neural tube formation reduction. The manuscript lacks a core message of the physiological importance of Par. Is Par critical of PSC maintenance? Is Par critical for neural system development?

Secondly, AKT-FURIN-..... axis still lacks supportive data. Various inhibitors were used to rescue the Par KO. But the link between each component in the axis is missing and rather superficial.

https://doi.org/10.7554/eLife.111448.1.sa1

Author response:

> ***Reviewer #1 (Public review):***
>
> *The study by He and colleagues aims to investigate the molecular mechanisms driving key cell potency transitions, particularly the naïve-to-primed pluripotency transition. The authors explore the relationship between cell polarity and stemness using stem cell models combined with a comprehensive panel of experiments, including pharmacological inhibition and co-culture/conditioned medium rescue approaches. Overall, the study provides interesting observations and contributes to the understanding of the molecular mechanisms dynamically regulating stem cell differentiation.*
>
> *However, several conceptual and interpretational aspects could be strengthened:*
>
> *(1) First, the Introduction would benefit from being more focused on what is currently known regarding cell polarity during early embryogenesis and pluripotent stem cell transitions, rather than emphasizing later neurogenesis events. Such reorientation would better match the main topic of the manuscript and improve the conceptual coherence of the study.*

We thank the reviewer for this constructive suggestion. We fully agree that the Introduction should be more tightly focused on the current understanding of cell polarity during early embryogenesis and pluripotent stem cell transitions, rather than on later neurogenesis events.

Accordingly, we will revise the Introduction in the following ways:

(1) Reduce the discussion on later neurogenesis and move some of those details to the Discussion section where they more appropriate.

(2) Expand the background on early embryonic development and pluripotent stem cell transitions by citing key recent and classical references, including but not limited to: cell polarity establishment in the preimplantation embryo, apical–basal polarity during lineage specification, polarity remodeling in naïve-to-primed pluripotent stem cell transition, the role of PAR complex in early mouse development.

(3) Refocus the Introduction to clearly state: what is known about polarity in early embryogenesis and pluripotent states, what remains unknown, and how our study addresses that gap.

> *(2) Similarly, Figure 6, where the authors attempt to provide clinical relevance through neural organoid formation experiments, feels somewhat disconnected from the central theme of the naïve-to-primed transition. Although this section is interesting on its own, there is already extensive literature describing polarization and morphogenetic events occurring much earlier during pluripotent state transitions. Therefore, the developmental*

> *relevance of the neural differentiation phenotypes could be better contextualized in relation to earlier morphogenetic events associated with pluripotency progression.*

We thank the reviewer for this insightful comment. We agree that the neural organoid experiments in Figure 6 are somewhat disconnected from the central theme of the naïve-to-primed transition, and that extensive literature already exists on polarization events occurring earlier during pluripotent state transitions.

In the revised manuscript, we will better contextualize these findings by explicitly discussing how the neural differentiation phenotypes relate to the earlier morphogenetic events associated with pluripotency progression, rather than presenting them as a standalone observation. We will also incorporate relevant references to bridge this gap and strengthen the developmental relevance of our neural organoid data.

> *(3) The manuscript contains a substantial amount of experimental work; however, several results would benefit from deeper discussion. For example, in Figure 1, what is the rationale behind ZO1 downregulation being observed specifically in primed PAR knockout cells but not under naïve culture conditions? In addition, in Figure 3, the authors perform co-culture and conditioned medium experiments between wild-type and knockout cells. While the authors focus on the secreted protein fraction that rescues the phenotype, they also mention that other fractions display rescuing activity. Could the authors briefly discuss what additional components may contribute to this rescue effect? For example, could other molecules within these fractions also converge on AKT signaling regulation?*

We thank the reviewer for recognizing the substantial experimental work in our manuscript and for providing these thoughtful suggestions to improve the depth of our discussion. We agree that deeper discussion of several key results will strengthen the manuscript. In the revised version, we will address the specific points as follows:

(1) Regarding ZO1 expression in Figure 1:

Our primary focus is actually on ZO1 localization rather than its total expression level. In our experiments, RNA-seq and immunofluorescence analysis revealed that the total expression level of ZO1 does not change significantly in PAR knockout cells. However, ZO1 localization is markedly altered in PAR knockout primed cells. Specifically, in wild-type primed cells, ZO1 is predominantly localized at the cell membrane, whereas this specific membrane accumulation is not observed in PAR knockout primed cells. Furthermore, this phenomenon is observed specifically under primed state and does not occur under naïve culture conditions. This is likely due to the differential requirement for PAR complex components in maintaining tight junction integrity during distinct pluripotency stages.

(2) Regarding the rescue activity of other fractions in Figure 3:

In our experiments, we found that beyond the secreted protein fraction, the WT CM-Exosome fraction exhibited limited rescue efficacy, particularly during the later stages of NPT. Based on our literature review, we suggest that these exosomal components may still contribute to the observed rescue effect, potentially through the delivery of functional proteins, miRNAs, or other signaling modulators that converge on AKT signaling regulation. This discussion will provide a more comprehensive understanding of the paracrine communication between wild-type and knockout cells, while acknowledging the limited contribution of exosomes relative to the secreted protein fraction.

> *(4) Importantly, transitions in cell potency are frequently associated with coordinated morphogenetic changes. For example, during mouse embryogenesis, naïve pluripotent inner cell mass cells progressively polarize into a rosette-like structure with apical domain specification before lumen formation and epithelialization during progression*

> *toward the primed epiblast state. This developmental context could help strengthen the biological interpretation of the study.*

We sincerely thank the reviewer for providing this valuable developmental context. The example of naïve pluripotent inner cell mass cells progressively polarizing into rosette-like structures with apical domain specification before lumen formation and epithelialization during progression toward the primed epiblast state is highly insightful and directly relevant to our study.

In the revised manuscript, in the Introduction section, we will incorporate this developmental perspective to strengthen the biological interpretation of our findings. Specifically, we will place greater emphasis on the role of Par complex-mediated cell polarity in coordinating both pluripotency transitions and morphogenetic changes during early embryogenesis. We believe this contextualization will significantly improve the framing of our study and better connect our *in vitro* observations to *in vivo* developmental processes.

> *(5) There are also several claims throughout the manuscript that appear to be overinterpreted or insufficiently quantified. For example, in Figure 1, the authors state that CDH1 expression is uniform; however, this is difficult to appreciate from the images shown, and quantitative analysis would be necessary to support this conclusion.*

We thank the reviewer for this important comment. We agree that the claim that "CDH1 expression is uniform" in Figure 1 is overinterpreted based on the images shown, and we apologize for the lack of quantitative support.

Upon re-examination, we realize that our focus should be on CDH1 localization rather than its expression level or uniformity. In the updated manuscript, we will rephrase the statement about uniformity and instead present appropriate quantitative analysis (e.g., RNA-seq or fluorescence quantification across multiple cells) to better support our conclusions regarding CDH1 distribution. We will also adjust our data presentation to more clearly reflect the localization changes we observe.

> *(6) Another example appears in Figure 2, where the authors claim that "heatmap analysis revealed that transcriptomic profiles of PAR knockout cells progressively diverged from wild type from day 3 onwards". This conclusion is not fully supported by the presented data for two reasons: (1) transcriptomic divergence is more appropriately assessed through principal component analysis, clustering, or distance-based methods rather than by visual inspection of a heatmap alone; and (2) although some genes displayed in panel E begin to show genotype-associated differences from day 3, the overall transcriptomic structure shown in the PCA and heatmap remains primarily dominated by temporal progression rather than genotype.*

We thank the reviewer for this careful and constructive critique. We apologize for the imprecise claim regarding the heatmap analysis in Figure 2. We agree that 1) transcriptomic divergence should be assessed by PCA, clustering, or distance-based methods rather than by visual inspection of a heatmap alone, and 2) the overall transcriptomic structure shown in PCA and heatmap remains primarily dominated by temporal progression rather than genotype.

In fact, our main point in this figure was to show that differentially expressed genes (DEGs) between PAR KO and WT become more numerous and more pronounced from day 3 onwards, and the supporting data for this claim are presented in Supplemental Figure 2 A–B. The number of DEGs between PAR knockout and wild-type cells is 480 at day 1, 523 at day 3, 1088 at day 4, and 1893 at day 6. Furthermore, we focused on specific genes within particular signaling pathways, and their expression levels began to show significant differences between PAR knockout and wild-type cells from day 3 onwards.

We realize that our original wording was misleading. In the revised manuscript, we will rephrase our conclusion to more accurately reflect what the data actually show, focusing on the timing and extent of differential gene expression rather than suggesting a global divergence of transcriptomic profiles.

> *(7) In this context, it remains unclear whether PAR knockout cells truly retain a more naïve pluripotent transcriptomic identity. To support this claim, the authors should compare the knockout transcriptome directly against a naïve pluripotent population. The phenotype observed in the knockout cells may instead represent an incomplete or aberrant primed transition rather than maintenance of naïve pluripotency itself. Intermediate morphogenetic states, such as rosette-like epithelial stages, could also explain the observed phenotype.*

We apologize for the confusion caused by our imprecise wording. We realize that our original manuscript may have inadvertently suggested that Par knockout cells retain a naïve pluripotent transcriptomic identity, which was not our intended claim.

To clarify, Par knockout naïve cells lose their naïve identity and differentiate toward a primed state during the NPT process described in this manuscript. Unlike wild-type primed cells, PAR-knockout primed cells exhibit altered morphology: they cannot establish or maintain the typical flat morphology, and possess distinct expression profile. In terms of naïve identity, key naïve markers (e.g., *Esrrb* or *Oct4*) are downregulated to comparable levels in both wild-type and Par knockout primed cells. Although the two cell types differ in their overall expression profiles, several core primed markers (e.g., *Fgf5* or *T*) show normal expression in both groups. Collectively, these results indicate that Par knockout naïve cells do lose their naïve identity and undergo differentiation toward a primed state during NPT, even though the final primed states of the two cell populations are distinct.

In the revised manuscript, we will:

(1) Revisit and revise our wording to avoid any misinterpretation that Par knockout cells retain a naïve identity.

(2) Directly compare the transcriptome of Par knockout cells against a true naïve pluripotent population (e.g., naïve ESCs) to further support our conclusion that the knockout cells are not maintaining naïve pluripotency, but rather exhibit an aberrant primed state with morphological abnormalities.

(3) Discuss the possibility that the observed phenotype may represent an intermediate morphogenetic state (e.g., rosette-like epithelial stages) rather than genuine naïve pluripotency maintenance.

> *(8) Strengthening this aspect of the study would substantially improve its developmental and in vivo relevance, which currently appears somewhat limited. In particular, it would be interesting to determine whether this mechanism operates during embryogenesis itself. The authors could consider relatively simple but informative experiments, such as perturbing PAR signaling or Furin activity during embryo culture.*

We thank the reviewer for this constructive and forward-looking suggestion. We agree that the current manuscript focuses primarily on *in vitro* cellular mechanisms, and we have not sufficiently explored the developmental and *in vivo* relevance of our findings. We acknowledge that this aspect of the study is currently somewhat limited.

In the revised manuscript, we will:

(1) Explicitly acknowledge this limitation in the Discussion section.

(2) Incorporate more background on early embryogenesis, particularly regarding pluripotency transitions and morphogenetic changes during early development, to better contextualize our *in vitro* observations.

(3) We will attempt to use embryo-like models to investigate whether the PAR complex–Furin–Lefty–FAK signaling axis also operates during embryogenesis itself. As the reviewer suggested, simple but informative experiments—such as perturbing PAR signaling or Furin activity during embryo culture—would be valuable next steps to determine the *in vivo* relevance of our proposed mechanism. We will include these as important future perspectives.

> *(9) Along the same lines, some statements in the manuscript appear overly speculative. For example, the statement that "these findings may reveal a developmental compensation mechanism during embryogenesis, whereby normal cells rescue defective cells or increase their own proportion" extends well beyond the experimental evidence presented. Such claims invoke concepts related to cell competition, abnormal cell recognition, or developmental quality control mechanisms in vivo, none of which are directly demonstrated in this study. The authors are encouraged either to substantially tone down these statements or move them to the Discussion as speculative possibilities.*

We thank the reviewer for this important critique. We agree that our original statement —"these findings may reveal a developmental compensation mechanism during embryogenesis, whereby normal cells rescue defective cells or increase their own proportion"—is overly speculative and extends beyond the experimental evidence presented in our study. We also acknowledge that it was inappropriate to directly extrapolate from *in vitro* cellular mechanisms to *in vivo* developmental rules without proper justification.

In the revised manuscript, we will:

(1) Substantially tone down this claim from the Results section.

(2) Move this speculation to the Discussion section, where we will explicitly present it as a speculative possibility rather than a conclusion supported by our data. We will also clearly state that concepts such as cell competition, abnormal cell recognition, or developmental quality control mechanisms remain to be tested in future studies.

> *(10) Another important conceptual point concerns the relationship between PAR complex regulation and Lefty signaling. If this mechanism indeed reflects a physiological or homeostatic process operating during embryogenesis, what would be the developmental rationale for the PAR complex regulation of Lefty? Lefty is well known for its role during gastrulation and anterior epiblast patterning. It would therefore be interesting if the authors could further discuss potential links between these developmental contexts.*

We thank the reviewer for raising this important conceptual point. In our manuscript, we have indeed demonstrated that the PAR complex regulates Lefty signaling under the conditions of this study, and we are aware from the literature that Lefty signaling plays a critical role during early embryogenesis, particularly in gastrulation and anterior epiblast patterning.

However, we admit that we have not deeply considered the potential pathways and developmental rationale for PAR complex-mediated regulation of Lefty in the context of embryogenesis. This is an important gap in our current discussion.

In the revised manuscript, we will:

(1) Review and incorporate relevant literature to better understand and discuss the potential links between PAR complex regulation and Lefty signaling during early embryonic

development, including possible connections to gastrulation and anterior patterning.

(2) Offer speculative but informed perspectives on the developmental rationale for such regulation, while clearly distinguishing between what our data directly show and what remains to be explored in future studies.

> *Minor points:*
>
> *(1) The authors state that PAR knockout cells do not exhibit major differences in self-renewal capacity; however, they simultaneously claim that these cells remain in a more naïve-like state. This interpretation requires clarification, as naïve pluripotent cells are typically associated with increased clonogenicity, enhanced self-renewal, and expression of markers such as alkaline phosphatase and SSEA1 compared to primed cells. The relationship between the observed phenotype and the proposed "naïve-like" state should therefore be discussed more carefully.*

We thank the reviewer for this comment, which addresses a similar concern as Point 7 mentioned above. Consistently, we do not claim that PAR knockout cells remain in a more "naïve-like" state. Our actual conclusion is that PAR knockout naïve cells undergo differentiation toward the primed state during NPT. However, due to loss of cell polarity, PAR knockout primed cells fail to establish and maintain the typical flat morphology and instead form dome-shaped colonies. Importantly, these dome-shaped colonies do not retain the characteristics of the naïve state, such as increased clonogenicity, enhanced self-renewal, or expression of alkaline phosphatase and SSEA1.

In the revised manuscript, we will:

(1) Revise our wording to avoid any misinterpretation that PAR knockout primed cells maintain a naïve-like identity.

(2) Explicitly clarify that the observed dome-shaped morphology represents an aberrant primed state rather than a naïve or naïve-like state.

(3) Discuss more carefully the relationship between the observed phenotype and the absence of typical naïve state features.

> *(2) The authors generated several independent knockout clones, but appear to use only one clone for downstream analyses after observing similar morphogenetic phenotypes. Is this sufficient to account for potential clonal heterogeneity? Would the use of pooled clones provide a more robust experimental system?*

We thank the reviewer for raising this important concern regarding clonal heterogeneity. We agree with the reviewer that our current approach using only one representative knockout clone for downstream mechanistic analyses after confirming similar morphogenetic phenotypes across multiple independent clones is not sufficient to fully exclude potential clonal heterogeneity.

To address this issue, we will perform additional experiments in the revised study. Specifically, we will use another independent knockout clone (ParKO6) to repeat the key mechanistic analyses. The following experiments will be carried out:

(1) ParKO6 and wild-type ESCs will be subjected to NPT. During the NPT process, cells will be treated with an AKT inhibitor (MK2206), a FAK inhibitor (PF562271), or WT CM. We will observe whether the morphological defects of ParKO6 cells are rescued, and RT-qPCR will be performed to characterize the molecular features of ParKO6 cells under these conditions.

(2) After treatment with the AKT inhibitor (MK2206), FAK inhibitor (PF562271), or WT CM, immunofluorescence (IF) will be used to detect p-FAK levels in ParKO6 cells.

(3) Following the same treatments, Western blotting (WB) will be performed to detect FURIN and LEFTY protein levels in ParKO6 cells.

These additional experiments will allow us to confirm that the observed results are not due to clone-specific artifacts from the originally used clone.

> *(3) The rescue experiments using pathway inhibitors are interesting; however, the interpretation again relies primarily on colony morphology. Readers may question whether these experiments truly represent rescue of the naïve-to-primed transition itself without additional transcriptomic or molecular characterization.*

We thank the reviewer for this important comment. We apologize for the lack of clarity in our original manuscript, which may have led to the misunderstanding that our interpretation of the rescue experiments relied solely on colony morphology.

In fact, we did perform molecular characterization on a subset of cells rescued by pathway inhibitors, and these data are presented in Supplemental Figure 2 D–E. We realize that our description of these results was insufficiently clear, and we failed to properly highlight this molecular evidence in the main text.

In the revised manuscript, we will revise our wording to clearly state that the rescue effects are supported not only by morphological observations but also by molecular characterization.

> *(4) In Figure 4, the manuscript could be strengthened by integrating transcriptomic analyses from pharmacological treatments with the secreted-factor and co-culture datasets.*

We thank the reviewer for this constructive suggestion.

In our current manuscript (Figure 4), we have indeed performed an integrated transcriptomic analysis comparing pharmacological treatment and secreted-factor treatment, and we demonstrated that both treatments converge on the FAK signaling.

Regarding the co-culture dataset, we did not include it in the integrated analysis presented in Figure 4. This is because, based on our data in Figure 3, we concluded that the rescue effect observed in co-culture is primarily mediated through secreted factors. Therefore, the secreted-factor transcriptomic data already capture the key signaling pathways responsible for the co-culture rescue effect.

We will clarify this rationale explicitly in the revised manuscript to avoid any confusion.

> *(5) The authors could better clarify the context of Furin downregulation in the knockout cells. Is this a direct consequence of altered transcriptional regulation by the PAR complex, or could it instead represent a secondary consequence of impaired progression through the primed pluripotent transition?*

We thank the reviewer for this important mechanistic question.

Based on our experimental data, we conclude that Furin downregulation in PAR knockout cells is a direct consequence of altered transcriptional regulation by the PAR complex, rather than a secondary consequence of impaired progression through the primed pluripotent transition. Our evidence is as follows:

(1) Transcriptomic analysis revealed that PAR knockout leads to a significant reduction in Furin RNA levels.

(2) Western blot analysis confirmed that PAR knockout also results in a significant reduction of FURIN protein levels.

(3) Importantly, treatment with an AKT inhibitor (upstream of the proposed pathway) significantly upregulated both Furin RNA and protein levels in PAR knockout cells. In contrast, treatment with a FAK inhibitor or WT CM (downstream) did not significantly alter Furin expression.

These data collectively indicate that Furin downregulation is directly linked to PAR complex-mediated transcriptional regulation, rather than being an indirect consequence of defective primed state transition. We will clarify this rationale in the revised manuscript.

> ***Reviewer #2 (Public review):***
>
> *Summary:*
>
> *The study demonstrated that Par, but not other polarity genes, Crumbs or Scrib, regulates cell polarity during PSC transition to primed state as well as neural tube formation.*
>
> *Strengths:*
>
> *The use of KO convinces the role of Par in NPT. Scrib and Crumbs KO data are informative to the field. The conditioned medium experiment is informative. They suggested the potential secreted factors over 50kDa are responsible for maintaining the polarity of NPT in Par KO.*
>
> *Weaknesses:*
>
> *(1) Most importantly, how Par is important for PSC maintenance and differentiation is not clear. The data provided are dome shape formation, endoderm lineage tendency, and neural tube formation reduction. The manuscript lacks a core message of the physiological importance of Par. Is Par critical of PSC maintenance? Is Par critical for neural system development?*

We thank the reviewer for this critical comment, which helps us better articulate the core message of our study.

In our manuscript, we have provided clear evidence regarding the role of the PAR complex in pluripotent stem cell (PSC) maintenance and differentiation:

(1) Regarding PSC maintenance:

The PAR complex is not critical for PSC maintenance under self-renewing conditions. Specifically, PAR knockout does not significantly affect the expression levels of pluripotency genes (Figure 1 B–C and Supplemental Figure 1 C). Moreover, PAR knockout PSCs can be continuously cultured for at least 30 passages without notable changes in cell morphology or proliferation capacity (Figure 1 D–F). These findings are consistent with previous literature, which demonstrates that the core function of the PAR complex is to establish and maintain cell polarity, rather than directly regulating the transcriptional network of pluripotency genes.

(2) Regarding PSC differentiation:

The PAR complex is important for proper differentiation. PAR knockout leads to multiple differentiation defects, including: Failure to establish normal cell morphology during (NPT) (Figure 1 G–K). Impaired formation of proper three-germ-layer structures during embryoid body (EB) and teratoma differentiation (Figure 5 F–G). In particular, the type and quantity of

ectodermal tissues are significantly reduced. Consistent with our findings, previous literature has reported that PAR complex deficiency leads to neural developmental defects in mouse embryos, resulting in mid-gestation embryonic lethality.

(3) Regarding neural system development:

The PAR complex is critical for neural development. During neural stem cell (NSC) differentiation, PAR knockout cells exhibit a significantly reduced efficiency of Nestin-positive cells and fail to form the classical rosette structures (Supplemental Figure 5 B–C). During neural tube organoid induction, PAR knockout cells show significantly impaired lumen formation and spontaneous elongation efficiency. Moreover, during subsequent maturation, PAR knockout cells fail to differentiate into neurons, leading to a marked reduction in neural tube organoid maturation efficiency (Figure 6 B–E).

These findings are consistent with previous literature showing that in zebrafish embryonic development, mislocalization of the PAR complex leads to neural tube abnormalities while PAR complex deficiency results in severe hydrocephalus; in mouse embryonic development, PAR complex deficiency causes neural developmental defects leading to embryonic lethality; and disruption of the PAR complex impairs the formation of apical tight junctions in the neuroepithelium and subsequent neuroepithelial tissue polarization, resulting in neural tube closure defects in humans.

In the revised manuscript, we will incorporate classical literature to discuss the essential roles of the PAR complex in early embryonic development, thereby providing a broader developmental context for our findings.

> *(2) Secondly, AKT-FURIN-..... axis still lacks supportive data. Various inhibitors were used to rescue the Par KO. But the link between each component in the axis is missing and rather superficial.*

We thank the reviewer for this critical comment. We acknowledge that the proposed AKT–FURIN–LEFTY–ECM-integrin–FAK signaling axis has certain limitations, particularly that the connection between LEFTY and ECM-integrin lacks direct experimental support. Therefore, in the revised manuscript, we will de-emphasize the role of ECM and integrin and revise the signaling axis to AKT–FURIN–LEFTY–FAK.

We believe the current data and previous publications support this revised signaling axis well. Accordingly, we have summarized the relevant information as follows. In addition, we plan to perform additional experiments to further support the new signaling axis, which are also included in the following text.

(1) AKT-FAK

We found that Par KO cells exhibit defects during NPT, and these defects can be rescued by AKT inhibitor (MK2206), FAK inhibitor (PF562271), and WT CM. Through transcriptomic analysis, we found that both AKT inhibitor and WT CM share similar expression profiles with WT and converge on FAK signaling. Notably, through Western blotting analysis, we found that Par KO led to upregulated p-AKT levels, which were effectively suppressed by MK2206 treatment, but WT CM did not decrease p-AKT levels. In contrast, through immunofluorescence analysis, we found that FAK signaling was hyperphosphorylated in Par knockout primed cells compared to WT primed cells, and MK2206, WT CM, and PF562271 all effectively reduced p-FAK levels. Given that both MK2206 and WT CM attenuated the elevated p-FAK, we propose that all three treatments restore the flat monolayer morphology by regulating FAK signaling homeostasis, with WT CM acting downstream of AKT signaling. The relevant data are presented in Figure 1G-I, Figure 2F, Figure S2C, Figure 3H-I, Figure 4A-D, and Figure S4A.

(2) AKT-LEFTY

Through integrated proteomic and transcriptomic analysis, we identified a set of functional proteins. Overexpression screening revealed that LEFTY exhibited the most significant rescue effect in Par KO cells during NPT. Proteomic analysis revealed that the protein levels of LEFTY were significantly higher in WT CM compared to KO CM, suggesting that WT cells modulate FAK signaling via secretion of LEFTY proteins. It is therefore reasonable to infer that MK2206 rescues the defects in Par KO primed cells through upregulation of LEFTY expression. Western blotting analysis confirmed this, showing that MK2206 significantly increased LEFTY protein levels in Par KO primed cells. The relevant data are presented in Figure 4E, Figure 4H and Figure S4C-D.

(3) LEFTY-FAK

Proteomic analysis indicated that WT CM treatment supplied extracellular LEFTY to Par KO ESCs, thereby rescuing the phenotypic defects of Par KO primed cells, and significantly reduced p-FAK levels in these cells. Concordantly, LEFTY overexpression also reduced p-FAK in Par KO primed cells. These results are consistent with the reported role of LEFTY in suppressing FAK signaling (Alowayed et al., 2016). The relevant data are presented in Figure 4D, Figure 4F, and Figure S4D-E.

(4) AKT-FURIN

LEFTY proprotein requires FURIN-mediated cleavage for secretion and function (Dubois et al., 2001). Through transcriptomic analysis, we found that Par KO downregulated Furin mRNA expression, while MK2206 treatment restored its expression levels. Through Western blotting analysis, we found that MK2206 increased FURIN protein abundance and cleaved LEFTY levels. The relevant data are presented in Figure 4G-H.

(5) FURIN-LEFTY

To validate the role of FURIN in LEFTY maturation, we treated WT cells with BOS318, a highly specific and potent inhibitor of FURIN that irreversibly binds to the protease by mimicking its natural substrate (Ivachtchenko et al., 2024). BOS318 induced WT primed cells to adopt a dome-shaped morphology resembling Par KO primed cells, confirming that inhibition of FURIN prevents LEFTY secretion and function, leading to defective primed cell morphology. The relevant data are presented in Figure 4I-J. To further strengthen the role of FURIN in regulating LEFTY, we will treat wild-type cells with BOS318 and examine the expression changes of LEFTY.

(6) ECM/integrin

Integrated analysis of both transcriptomic and proteomic data revealed that Par KO leads to significant enrichment of pathways associated with ECM and integrin (Figures 2D, 3F, 3K, and S4B). Notably, both MK2206 and WT CM treatment co-upregulated the ECM-receptor interaction pathway (Figure 4C). The FAK signaling pathway serves as a central node that integrates upstream inputs from both PKC and AKT pathways while transducing extracellular cues derived from ECM-integrin interactions into intracellular signaling cascades (Sakthivel et al., 2025). We therefore propose that secreted LEFTY acts as an extracellular signal that activates specific ECM receptors and modulates integrin complexes, thereby regulating FAK phosphorylation and maintaining normal cell adhesion and morphology. However, this speculation still lacks direct experimental evidence. We will endeavor to perform additional experiments to support this proposed connection in the future. Nevertheless, we have decided to de-emphasize the role of ECM and integrin in the AKT–FURIN–LEFTY–FAK signaling axis in the current manuscript.

References

Alowayed, N., Salker, M. S., Zeng, N., Singh, Y., & Lang, F. (2016). LEFTY2 Controls Migration of Human Endometrial Cancer Cells via Focal Adhesion Kinase Activity (FAK) and miRNA-200a. Cellular Physiology and Biochemistry, 39(3), 815-826. *https://doi.org/10.1159/000447792*

Dubois, C. M., Blanchette, F., Laprise, M.-H., Leduc, R., Grondin, F., & Seidah, N. G. (2001). Evidence that Furin Is an Authentic Transforming Growth Factor-β1-Converting Enzyme. The American Journal of Pathology, 158(1), 305-316. *https://doi.org/10.1016/s0002-9440(10)63970-3*

Ivachtchenko, A. V., Khvat, A. V., & Shkil, D. O. (2024). Development and Prospects of Furin Inhibitors for Therapeutic Applications. International Journal of Molecular Sciences, 25(17). *https://doi.org/10.3390/ijms25179199*

Sakthivel, K., Kotowska, A., Fan, Z., Portner, E. J., Merry, C., Nordenfelt, P., Simonsen, A. C., Wright, A. J., & Swaminathan, V. S. (2025). Integrin-Piezo1 Axis Drives ECM Remodeling and Invasion of 3D Breast Epithelium. Advanced Science. *https://doi.org/10.1002/advs.202509932*

https://doi.org/10.7554/eLife.111448.1.sa0